AMERICAN UNIVERSITY OF BEIRUT

THE EFFECT OF NANO-ROUGHNESS OF NEURAL IMPLANTS ON CELL GROWTH, PROLIFERATION AND ADHESION OF HUMAN NEURONS AND GLIA

by
RIMA WADIH LAHOUD

A thesis
submitted in partial fulfillment of the requirements
for the degree of Master of Science
to the Department of Biomedical Engineering
of the Faculty of Medicine and the Maroun Semaan Faculty of Engineering and Architecture
at the American University of Beirut

Beirut, Lebanon
May 2021

AMERICAN UNIVERSITY OF BEIRUT

THE EFFECT OF NANO-ROUGHNESS OF NEURAL IMPLANTS ON CELL GROWTH, PROLIFERATION AND ADHESION OF HUMAN NEURONS AND GLIA

by

RIMA WADIH LAHOUD

Approved by:

Dr. Massoud Khraiche, Assistant Professor — Chair

Biomedical Engineering

Dr. Marwan El-Sabban, Professor — Co-Advisor

Anatomy, Cell Biology and Physiological Sciences

Dr. Firas Kobaissy, Associate Professor — Member of Committee

Biochemistry and Molecular Genetics

Firas Kobaissy

Digitally signed by Firas Kobaissy
DN: cn=Firas Kobaissy, o=American University of Beirut, ou, email=fk02@aub.edu.lb, c=US
Date: 2021.05.11 09:10:25 -04'00'

Dr. Mutasem Shehadeh, Associate Professor — Member of Committee

Mechanical Engineering

Mutasem Shehadeh

Date of thesis defense: May 4, 2021

AMERICAN UNIVERSITY OF BEIRUT

THESIS, DISSERTATION, PROJECT RELEASE FORM

Student Name: Lahoud (Last) Rima (First) Wadih (Middle)

☑ Master's Thesis ○ Master's Project ○ Doctoral Dissertation

☑ I authorize the American University of Beirut to: (a) reproduce hard or electronic copies of my thesis, dissertation, or project; (b) include such copies in the archives and digital repositories of the University; and (c) make freely available such copies to third parties for research or educational purposes.

☐ I authorize the American University of Beirut, to: (a) reproduce hard or electronic copies of it; (b) include such copies in the archives and digital repositories of the University; and (c) make freely available such copies to third parties for research or educational purposes after: **One ___ year from the date of submission of my thesis, dissertation or project.**
Two ___ years from the date of submission of my thesis , dissertation or project.
Three ___ years from the date of submission of my thesis , dissertation or project.

Rima Lahoud — Signature

May 11, 2021 — Date

This form is signed when submitting the thesis, dissertation, or project to the University Libraries

Acknowledgements

I would like to thank my advisor, Dr. Massoud Khraiche for his guidance during my research and studies at his lab. The experiences I gained introduced me to the world of biomedical engineering and they will remain with me forever.

I would also like to thank my co-advisor, Dr. Marwan El-Sabban for offering me the time and support. His many advice were always straightforward and on point.

I would like to acknowledge my committee members Dr. Firas Kobaissy and Dr. Mutasem Shehadeh and thank them for giving me beneficial suggestions and advice.

Last but not least, I would like to thank Dr. Wassim Abou Kheir for providing me his lab and resources to complete my experiments.

To my family, thank you for the love and support.

An Abstract of the Thesis of

Rima Wadih Lahoud for Master of Science
Major: Biomedical Engineering

Title: The Effect of Nano-Roughness of Neural Implants on Cell Growth, Proliferation and Adhesion of Human Neurons and Glia

Adhesion of neurons and glia to the surfaces of brain devices governs stimulation and recording efficacy and implant life. Nanotopography allows cells to interact with implants on a physical scale similar to that of its proteins and lipids leading to improvement in cell/substrate adhesion. For neural interfaces, a strong neuronal adhesion to the recording or stimulating sites on implanted devices provides close proximity of the neurons to the device and, therefore, yields a improved electronic signal transduction. The cell/substrate interaction involves several cellular mechanisms including biomechanical and biochemical changes in the cell. The emergence of new biomaterials and advances in nanofabrication techniques has enabled fine control over substate topography. In this work, we investigate the impact of Nanotopography on biochemical and biomechanical aspects of neural and glial cellular adhesion. We used polyimide as a substrate for adhesion, a common material for brain devices, and we developed a process that allows us to control its surface roughness on the nanoscale. We used SH-SY5Y Cells (Neuroblastomas) and human astrocytes (glia) cell line in our adhesion assays. Our results showed that SH-SY5Y and glia cell growth, proliferation and adhesion was best achieved at surface nano-roughness values around 8 and 4 nm, respectively. We also observed a relationship between adhesion force and surface roughness measured via a unique single cell force spectroscopy technique. The results sheds light on the impact of on cell adhesion and provides a guide for the ideal range surface roughness for implanted devices for both glia and neurons.

Contents

List of Figures

List of Tables

Chapter 1

Introduction

1.1 Objective

Cellular adhesion is intertwined with fundamental cellular functions whose properties can drastically change in the case of diseases; moreover, cellular adhesion to a substrate is a crucial player in the application of biomedical devices. Studying cell adhesion in conditions that mimic the extracellular matrix provides a better understanding of how the cells interact with their environment. One of the characteristics of an extracellular matrix and its components is its topography and geometrical features that form a nano-roughened structure for the cells to grow. A well-established cell-matrix adhesion process is essential for the proper development and survival of a cell. During development, a neuron searches for contact points or adhesion cues for the guided axon to make the necessary connections and migration to proper locations. One parameter that can increase the contact area of a substrate and shape its topography is nano-roughness. Finding a value of surface nano-roughness that encourages strong cell-substrate adhesion improves the design of cell culture vessels and allows the interpretation of experimental data to have a closer approach to how the cells intrinsically live.

An attractive material of choice for its high biocompatibility and unique characteristics is polyimide, a polymer made of imide monomers. It has a high thermal stability, chemical resistance and mechanical strength. Its dielectric properties have allowed it to be commonly used in medical devices and implants. In an effort to ameliorate the effectiveness of this material design, an oxygen plasma etching process was implemented to alter the surface nano-roughness of a polyimide substrate and increase its acceptance to cells. Following the activation process of the biomaterial, the cells were able to wet, spread and adhere shortly after getting in contact with it. The modified polyimide substrates were compared with conventional tissue culture plastic, which have relatively low surface nano-roughness values, to determine if higher surface nano-roughness values increase

the cell density of attachment.

1.2 Background

1.2.1 Importance of Cell Adhesion in Biomedical Applications

At present, many biomedical applications such as the utilization of implantable materials and the study of diseases often require an efficient cell adhesion for a better implementation of the application of interest and a good representation of the true cellular response. Cell adhesion maintains cellular integrity and structure that define the active processes and interconnected mechanisms involved in cell growth, survival, migration and differentiation [1]. An adequate cell-substrate adhesion strength allows the transduction of information from the surrounding microenvironment across the plasma membrane through the focal adhesion complex [2]. A change in the adhesion events can often be a sign of an underlying pathological condition, such as carcinogenesis [3]. Increasing the adhesion of a cell reduces its ability to detach, migrate, invade and metastasize. Some approaches depend on the cell adhesion phenomenon for cell sorting, where they use the selective adhesion of desired cell types to isolate them from other cell types in the same mixture of cells [4]. In a label-free device, the topographical features separated healthy cells from cancer cells based on their initial adhesion property [5]. Modification of surface topography can be achieved by random morphology or precise patterning techniques.

In neural interfaces, good physical, chemical and biological properties of the device allow it to record and stimulate target neurons in an accurate and non-invasive manner [6]. In vitro, materials with different surface roughness values modulated cellular growth and adhesion [7, 8]. Even repelling some cell types can be useful in targeting the attachment of the desired cell type. The proximity of a targeted neuron to the recording or stimulating device defined the efficiency of the interface [9]. An efficient neural interfacing device would minimize the probability of a foreign body reaction and maintain a close contact with viable target neurons. Glial recruitment and reactive gliosis are common indicators of device performance and have the ability to reshape the neural circuitry [10, 11]. Improved neural adhesion to the implantable device signifies greater acceptance of the device and minimizes its encapsulation over time. As the distance between the electrode and neurons increases, the amount of current needed to be delivered increases, and the amplitude of the response decreases. Relatively high current magnitudes delivered to target neurons could cause tissue damage and affect the performance of the electrode [12]. An electrode design that favors strong neural adhesion and growth to the device directly after implantation establishes a

strong junction between the neuron and the electrode. A stable long-term neuro-electronic junction would communicate more efficiently without deforming the neural cells. An intimate contact between the excitable tissue and the implanted electrode improves signal quality and maximizes the activation of neurons [13]. In addition, rough substrates have been shown to decrease the impedance of the electrode/electrolyte interface [14]. The signals recorded from the target neurons should be closely similar to the cells true electric activity, and the delivered signals for stimulation should reach them similar to the applied parameters.

1.2.2 Roughness Parameter in Neural Interfaces

The neuron-electrode interaction can be characterized by a circuit model that incorporates the physical parameters of the interface.

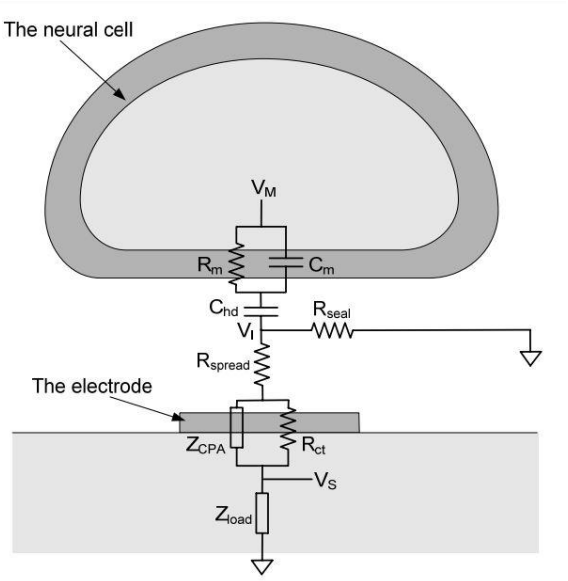

Figure 1.1: **Neuron-Electrode Interface Circuit Model.** Image taken from [15]. C_m, R_m and V_M are the cell membrane capacitance, resistance and potential, respectively. V_I and V_S are the voltages representing the neuron-electrode interface and the sensed potential, respectively. C_{hd} is the capacitance of the electrode. R_{seal}, R_{spread} and R_{ct} are the resistances corresponding to the gap between the neuron and the electrode, remaining spreading and charge transfer, respectively. Z_{CPA} and Z_{load} are the impedance parameters for the constant phase and the load, respectively.

Etching or the process of increasing the roughness property of an electrode in-

creases its active surface area and subsequently decreases electrode impedance [16]. As a general view to the model, the roughness parameter cannot be directly seen to affect impedance. Nevertheless, the resistance R_1 is related to the area A in equation 1.1

$$R_1 = x/kA \tag{1.1}$$

where x is the material thickness and k is the conductivity.
The impedance is correlated to the capacitance of an ideal capacitor, according to equation 1.2.

$$Z = 1/j\omega C \tag{1.2}$$

where ω is the perturbation frequency. Also, the double layer capacitance C_{dl} is dependent on the area in euqation 1.3:

$$C_{dl} = \varepsilon\varepsilon_0 A/d \tag{1.3}$$

where ε is the dielectric constant, ε_0 is the free space permittivity and d is the thickness of the double layer. Since the total impedance is calculated from real and imaginary components, the circuit model of a non-coated electrode can be modelled by equatin 1.4:

$$|Z| = \sqrt{R_1^2 + (\frac{d}{\omega^a \varepsilon\varepsilon_0 A})^2} \tag{1.4}$$

where a is less than 1 in a non-ideal capacitor. This equation provides a direct relationship between the electrode impedance and its active surface area [17].

1.2.3 Biocompatible Materials

The interactions between a non-living material and a living tissue can yield favourable or detrimental effects. An artificial material destined to work in or with a biological system is labeled as a biomaterial. In the absence of damaging effects, a biomaterial is considered a biocompatible material that can be used in a biological application. When a material is able to deliver satisfactory functioning and perform in the intended appropriate manner with the host, it then achieves biocompatibility. It should also not exhibit properties that are able to damage the cellular or living tissue; therefore, it should not be toxic nor induce undesirable reations. The selection of an appropriate material for use in a biomedical application or a medical device, the safety assessment of that material is necessary [18].

Organic materials, and more specifically polymers, have been attractive materials for the use in biomedical applications for their ability to regulate cellular functions [19, 20]. Biocompatible organic electrode coatings presented a soft

substrate that reduced the mechanical mismatch with the neural tissue. Some organic materials, like conductive polymers and carbon nanotubes, were able to allow safe electrical stimulation and avoid cell damage with undesirable chemical reactions such as hydrolysis [21]. Polymers are generally soft, which allows their topographies to be modified under stress. The effect of altering their surface topography has been examined on a variety of cell types to see their responses. It is common to have different cells respond distinctly to the same polymer surface morphology, which allows for the selective mediation of cellular mechanisms. A certain topography can encourage the adhesion and growth of a particular target cell while suppressing the activities of another, depending on the application.

Polyimide material is a polymer of imide monomers with a good thermal stability, chemical resistance, mechanical strength and flexibility [22]. Our study used the classic polyimide film called Kapton that results from the condensation of pyromellitic dianhydride and 4,4'-oxydianilin [23]. Polyimide can withstand temperatures ranging from -73°C to 260°C. Its material behavior did not change under temperature conditions similar to the physiological conditions of cells and body at 37°C, and its long-term stability makes it ideal for use in implantable devices[24, 25]. When used in the bio-integration of a neural implant for six months, the density of nerve fibers remained unaffected, and only a mild tissue reaction was observed after removing the implant [26].

One material of interest called graphene is a monolayer of carbon atoms arranged in a honeycomb structure. Graphene is a chemically stable material with unique mechanical and electrical characteristics and was found to be suitable for neural cell cultures [27]. This carbon-based nanomaterial preserved the cellular integrity of neural cells and enhanced cellular attachment [28]. Even so, purified retinal ganglion cells survived on bare graphene substrates without the addition of accommodating peptides, where the addition of a peptide coating did not alter the survival rate of neurons [29]. Graphene based substrates did not alter the excitability of target neurons and were suitable for use in biosensors and neurosthetic devices without the need of adhesion-promoting peptides [30]. Moreover, graphene reorganized the extracellular ions around the neural interface to increase neuronal firing and communication[31].

Poly(3,4ethylenedioxythiophene):poly(styrenesulfonate) (PEDOT:PSS) is an organic material suitable for neural interfacing since it reduced the electrochemical mismatch between the electrodes and cellular tissue, provided oxidative stability and achieved both electronic and ionic conductivity [32]. This organic material maintained high cell viability in vitro and showed good in vivo performance [33]. An ultraconformable and biocompatible neural interface that used PEDOT:PSS caused minimal damage to brain tissue due to its ability to conform to the topography of the brain tissue [34]. For the development of a neural interface device,

PEDOT:PSS could be printed on a biocompatible polyimide layer in a simple method [35].

1.2.4 Plasma Etching

Plasma etching offers precise etching at the nanoscale for material fabrication of biomedical devices. It limits the possibility of material contamination and does not require the use of hazardous chemicals during the etching process. Different materials react at different rates during the treatment process, where organic materials usually undergo change at a higher speed than inorganic materials [36]. Plasma treatment is an attractive technology for modifying the surface chemistry of polystyrene [37, 38] and microfluidic devices [39]. Oxygen plasma treatment is a common type of dry etching that increases the oxygen content of the surface of a polymer while increasing its hydrophilicity and changing its topography. This method can increase the surface energy of the substrate; however, it was found that substrates with high surface energy are detrimental to cell adhesion [40]. Polystyrene surfaces modified with oxygen plasma improved cell adhesion and proliferation [41]. To understand the interplay between plasma etching and surface roughness, we used the oxygen plasma approach to etch polyimide substrates. Atomic oxygen abstracts hydrogen and unsaturated moieties from the polymer surface while the saturated radicals weaken the C-C bonds [42]. Oxygen-based plasmas are well known to etch and roughen the polyimide surface while manipulating vacuum pressure [43] to become more adhesive in microelectronics [44]. Plasma treatment was compared with the ultraviolet-ozone cleaning method to assess its influence on the surface energy. Autoclave is another cleaning process that can modify and deteriorate the surface characteristics of a material, so it was not applied for polyimide.

1.2.5 Cell-Substrate Adhesion

The neural extracellular matrix is a highly structured environment with a mixture of molecules enabling them to grow and establish their extensions. Both types of cells inside the brain, the neurons and glia, manufacture and secrete mainly Hyaluronic Acid, which are in the glycosaminoglycans family, aggregan, neurocan and brevican, which are proteoglycans, and Tenascin-R, which is a type of glycoproteins [45]. Neurons can interact with their local environment and surrounding cells that have distinctive topographies ranging from the nanometer-scale to the micrometer-scale. Unlike other cells derived from epihelial, connective or muscle tissue, neurons have the ability to explore the extracellular matrix to make the necessary connections [46]. Cells can sense these topographical features as external stimuli and transduce their force signals into internal chemical signals that impact several cellular machineries [47]. They can respond to changes in the mechanical cues of an underlying substrate by changing their structure and

function accordingly [48].

Neural adhesion is a fundamental biological process and has crucial roles in brain development and neural interfacing. It involves highly coordinated intracellular signaling pathways that regulate cellular migration and differentiation during the developing brain and describes the interactions between numerous neurons and the interactions of neurons with their external environment. During neural development, axonal elongation from the growth cone depends on the adhesion to the substrate [49]. The mechanism of adhesion involves several complex pathways and can influence almost all aspects of cell survival, proliferation and behavior. Anchorage dependence or the attachment of a cell to a substratum ensures its survival and proliferation in appropriate situations. Substrates with large surface areas allow cells to form multiple adhesion sites in order to spread better, survive longer and proliferate faster [50].

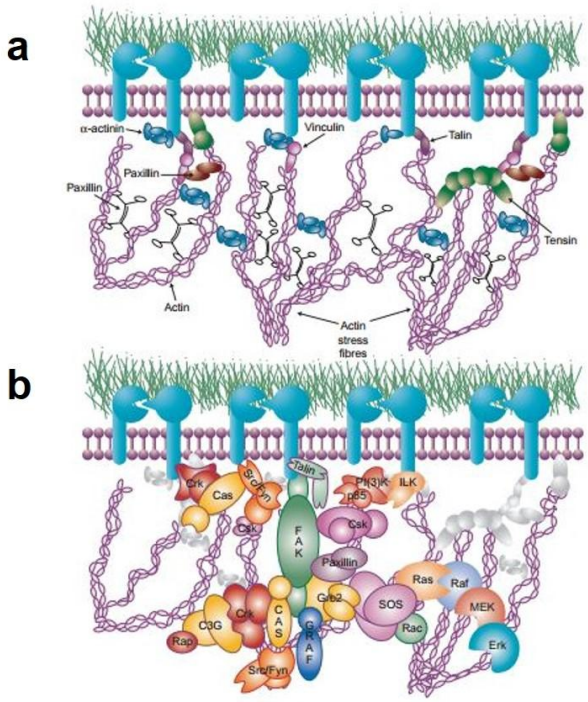

Figure 1.2: **Cytoskeleton Proteins.** (a) Proteins associated with integrin. (b) Signaling network that includes FAK and other molecules activated by integrin. Image taken from [2]

Cell attachment is orchestrated by an association of proteins in the focal adhesion that form a linkage to the cytoskeleton and surround the intracellular

tail of integrin. The integrins are the principal matrix receptors connecting the extracellular matrix to the interior cytoskeleton, as seen in Figure 1.2. These transmembrane adhesion molecules, which consist of two non-covalently bonded glycoproteins α and β, can send messages across the cell membrane in a bidirectional manner. The Focal Adhesion Kinase controls integrin signaling through tyrosine phosphorylation pathways and depends on the recruitment of intracellular anchor proteins. Through Focal Adhesion Kinase, activated integrins influence global cell responses and affect gene expression. One component of integrin signaling is the multidomain protein paxillin that helps in mediating reorganization of the cytoskeleton through its phosphorylation. It can be phosphorylated by FAK and can recruit signaling molecules to strengthen the adhesion complex. Proper assembly and disassembly of anchor proteins is necessary for the establishment of adhesion. Any change in the pathways involved in focal adhesions affects the cellular attachment or motility [51]. However, the exact biological processes behind these neuronal responses are not well understood [52].

1.2.6 Cell Adhesion Force Quantification Techniques

Several approaches have been employed for the quantitative analysis of cell adhesion. Centrifugation assays analysed the detachment forces of a large population of cells in a simple and convenient technique [53]. Surface plasmon resonance evaluated the dynamics of cell adhesion with high accuracy and temporal resolution [54]. Microfluidic shear force assays determined the critical shear stress force required to detach adherent cells in response to alterations of applied stress [55]. Mathematical models quantified the mechanical parameters underlying cell adhesion and related them to cell's intrinsic properties [56]. Atomic Force Microscopy (AFM) presents a scanning probe technology for the analysis of fixed or living biological samples at high resolution. It has been extensively used to measure and exert precise forces ranging from the piconewton to the nanonewton scale on cells to study their mechanical response. AFM uses a flexible cantilever that sweeps surfaces of interest several times horizontally through two modes. When the cantilever tip gets in contact with the surface, the tip traces its height. When it bends on the surface, the deflection value recorded by a laser beam determines the force applied on sample. Since the scanning force should remain constant during cantilever movement, a piezo system gives feedback and modifies cantilever position when needed [57]. However, standard AFM single cell force spectroscopy (SCFS) methods are time-consuming and yield low data output.
Fluidic Force Microscopy is a novel protocol useful for the quantification of adhesion force. It is based on the AFM setup in addition to fluid-filled microchanneled cantilevers. The cantilever tip has a microscale aperture that allows it to attach to a target cell by applying a negative pressure inside its microchannel. One study combine this robotic system with a label-free optical sensor to increase throughput and analyze the kinetics of adhesion in 30 individual cells [58].

The force spectroscopy principle is based on the deflection of the cantilever screened by a detector and taken as a voltage value (V) [V]. The measurement of the sensitivity of the cantilever to a hard substrate evaluates S [nm/V]. The voltage to distance relations is determined by the compensation of the cantilever movement of the piezo. The system then derives the force $F[N]$ from the following equation 1.5:

$$F = VSk \tag{1.5}$$

where k is the spring constant that is calculated according to Sader's method [59] in the equation 1.6:

$$k = \frac{Ewt^3}{4L^3} \tag{1.6}$$

which gives its relationship with the elastic modulus E [Pa], cantilever thickness t [m], width w [m] and length L [m]. Common cantilevers are 200-500 μm long, around 50 μm wide and 1 μm thick. By convention, positive forces are repelling forces while negative forces are attracting forces.

Interactions between the AFM tip and an object of interest are the resultant of one or more of the van der Waals, electrostatic, double layer, and capillary and adhesive forces. Van der Waals forces are the attractions between a slightly positive charge of one molecule and the slightly negative charge of another. In the AFM system, as the catilever tip is approaching the sample surface, the separation distance between the two is decreasing, making these type of interactions greater. Before the tip touches the surface, the forces are repulsive. When the tip lands and then bends on the surface, the forces become attractive. These forces are present in all materials, even the electrically neutral ones; however, they are considered as negligible in the presence of electrostatic forces. When imaging under an aqueous media, the negatively charged AFM substrate attracts positively charged ions in the aqueous solution. The oppositely charged ions accumulate at the solid-liquid interface and form what is known as a double layer. A solution with a relatively larger positive charge result in a lower electrostatic repulsion when the AFM tip approaches the sample placed in aqueous media. When imaging in air, the small radius of curvature of the AFM tip makes the tip an ideal location for water vapor condensation. By capillary action, the AFM tip with condensed water vapor droplets will consequently be pulled down further to stick to the surface [60].

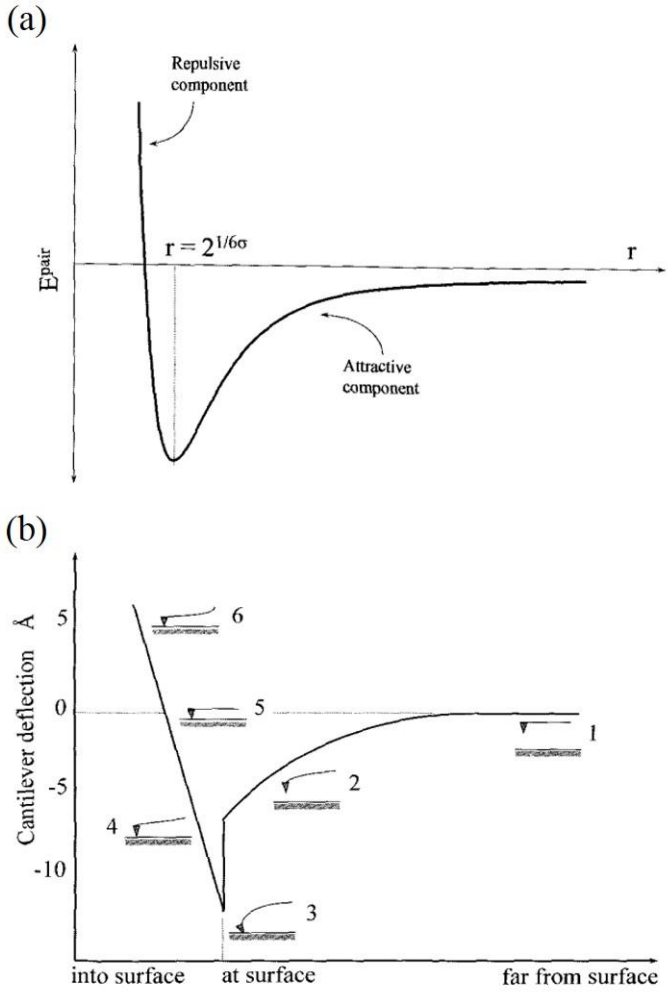

Figure 1.3: **Surface-AFM Force Interactions** (a) Graphical representation of the potential energy (E_{pair}) variation as a function of the separation distance between the pair (r) (b) Schematic representation of the ideal AFM cantilever state during its deflection process on the force-distance curve. When the tip is damaged, it deflects to position 6. [60]

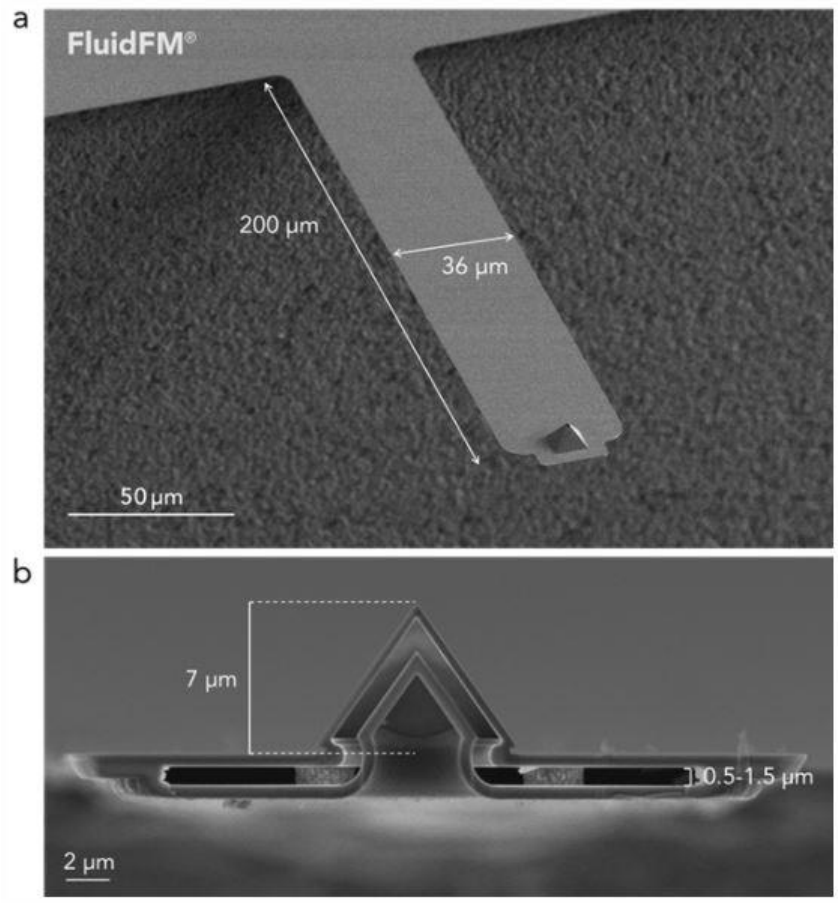

Figure 1.4: **Microscope Images of the Probe Geometry of a Nanopipette with an Aperture of 800 nm. This kind of probe tip is often used in FluidFM nanolithography experiments.**

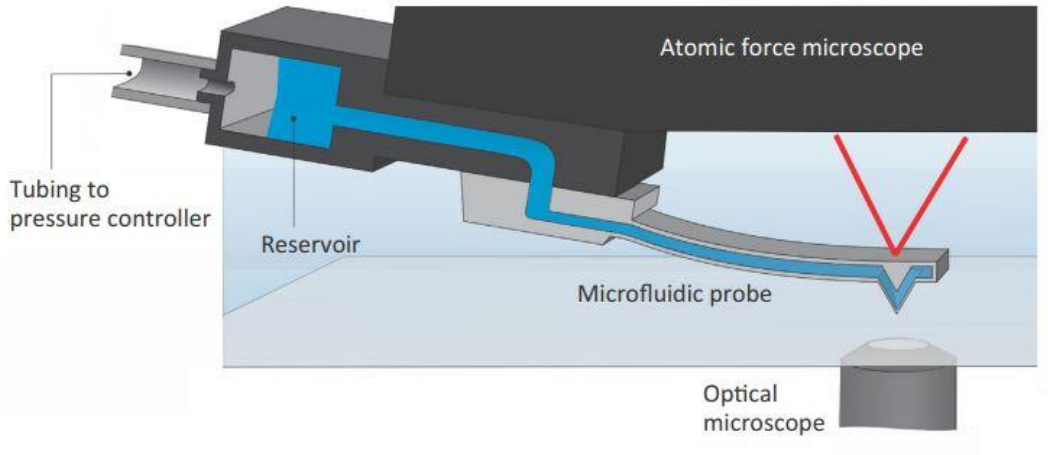

Figure 1.5: **Schematic Representation of the FluidFM System Setup. FluidFM combines AFM technology with a microfluidic system situated on top of an inverted microscope.** Image taken from [61]

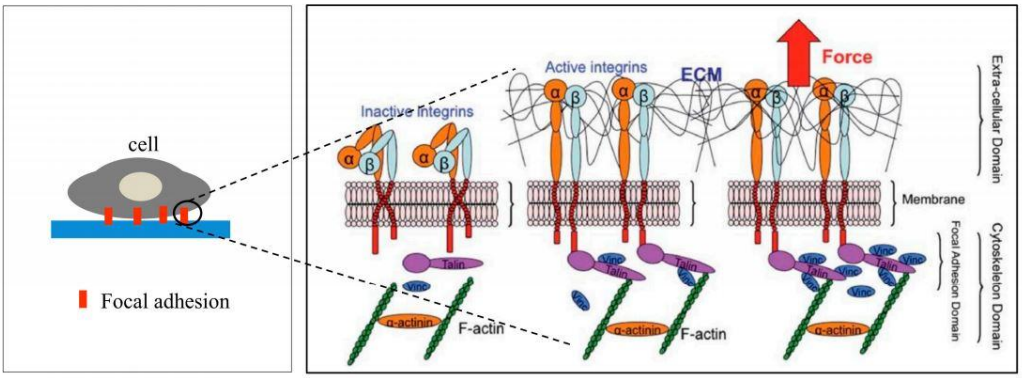

Figure 1.6: **Schematic Representation of the FAK Complex and Cytoskeleton Linkages Upon a Tensile Load Application** Image taken from [62, 63]

Chapter 2

Literature Review

2.1 Adhesion of Neuroblastoma Cells on Nanotopographies

Several studies show that substrate material with roughened surfaces can increase cellular attachment and, therefore, provide a much more suitable interfacing surface. To have a significant change in cellular attachment, substrate surfaces should have features with sub-microscale dimensions rather than microscale dimensions[64]. Rough or grooved substrates can have a specific pattern or a more random topography. Some substrates aim to replicate the geometry of the extracellular matrix components. A biomimetic replica of a glia cell surface allows a greater neural attachment as compared to a flat substrate of the same biomimetic material [65]. The surface morphology and properties of glia cells can thus dictate the neural growth behavior [66]. Current research focuses on finding the substrate material and design that promotes cellular growth and adhesion. Cell types differ in the structural and behavioral changes they undergo when exposed to a range of topographies [67].

Since cell-substratum adhesion is primarily integrin-based, Arnold et al. showed that surface roughness values above 73 nm allowed the proper arrangement and activation of integrin molecules and limited cell spreading [68]. The contact formation of integrin subunits with the substrate required features with a size of 140 nm while cell spreading required them to be at 440 nm [69].

Brunetti et al. investigated the response of SH-SY5Y cells to nanorough surfaces and demonstrated that these cells had a high sensitivity to variations in the surface roughness values at the nanoscale. At roughness values of 35 nm and above, the percent of adherent SH-SY5Y cells greatly decreased while the percent of necrotic cells greatly increased. The cells on the nanorough substrates lost their neural polarity and changed their ordered organization of their actin cy-

toskeleton. The sensitivity of the focal adhesion to the surface roughness caused the decrease in cell adhesion and triggered a cascade of events that eventually lead to necrosis [70].

Parikh *et al* investigated the cell spreading and cytoskeleton of SK-N-SH neuroblastoma on three nanoroughened ceramic surfaces: islands with 36 nm feature size and 55 nm spacing, connected islands with 57 nm feature size and 66 nm spacing, and pits with 36 nm feature size and 124 nm spacing. On smooth substrates, the cells spread in a similar manner to those on control tissue culture polystyrene. The SK-N-SH cells cultured on connected islands and pits exhibited greater polarity, which is an indicator of strong adherence; whereas, those cultured on islands doubled their cellular area. Cells achieved very limited spreading on the pits substrates but notable spreading on the connected surface. The clustered actin and vinculin cytoskeletal proteins expression in SK-N-SH cells grown on the smooth, connected and pits substrates confirmed the formation of a well-developed focal adhesion complex. Furthermore, the connected islands topography provided a greater focal contact for the cells [71].

Neuro-2A mouse neuroblastoma cells were cultured on modified silicon chips and were found to adhere tightly to the porous surfaces more than the flat substrates. They clustered into small worlds on the nanoroughened surfaces in a similar manner in which neurons form networks to maximize communication. Even after plating the substrates with the same cell density, flat surfaces provided less anchorage points which lead to a reduction in cell density after 24 hours in culture. The number of adhered Neuro-2A cells increased with the increase of surface nanoroughness values, with the sharp increase at substrates with 75 nm features [72]. Neuro-2A cells cultured on surfaces with large pores ranging from 1000 nm to 3000 nm were unable to find anchorage points and relied on intercellular contacts for survival. On porous surfaces ranging from 100 to 300 nm, these cells did not achieve their optimal adhesion ability. On surfaces with 50 nm to 100 nm feature size, the cells were able to form clustering but exhibited a spherical morphology. Only at pore size less than 50 nm that the Neuro-2A were able to exhibit their typical morphology[73]. These neuroblastoma cells were also able to achieve clustering and small-network properties at surface roughness values of 20 nm [74].

The murine PC-12 cells showed normal cell morphology, organization and differentiation on zirconia surfaces with a specific roughness parameter of 15 nm. Another zirconia surface with 25 nm roughness did not provide enough biophysical cues for the complete neuritogenesis of the PC-12 cells [75]. Nanotopography affected neural differentiation and neuritogenesis and even guided them in some cases. Upon differentiating PC-12 cells, NGF increased intercellular adhesion of these neural-like sympathetic cells and increased their adhesion with the substrate [76]. Normally, the PC-12 cells required NGF concentration of 50 ng/mL to opti-

mally extend their neurites. However, at sub-optimal NGF concentrations of 5 to 25 ng/mL, nanotopographies took a greater control of the PC-12 neuritogenesis. On flat surfaces, only 17% of the PC-12 cells maintained in a NGF concentration of 25 ng/mL formed neurites in contrast to 54% of the ones maintained in 50 ng/mL. On surfaces with ridges of 70 nm and 250 nm, neurite formation rose to 121% of the flat surfaces [77]. The material of the rough substrates under use had an influence on PC-12 NGF differentiation where graphene enhanced neurite length and allowed standard neuronal differentiation and cell viability [78].

Change in adhesion function influenced by surface topography and roughness was also observed in neural cultures. Several types of neural cells adhered differently to distinct surface topographies and more specifically surface roughness values. Primary cortical cells adhered optimally on substrates with surface roughness values ranging from 20 to 100 nm after 6 days in culture. On surfaces with 64 nm roughness, these neurons reached the greatest covered surface area; whereas, on surfaces with lower or higher roughness values, the cell density and adherence were lower than their normal or optimal values [79]. Neuronal behavior and neural network structure changed on flat vs. rough surfaces. Corrugated silicon surfaces with low roughness values of around 22 nm enhanced the clustering of primary neural cultures. The so-called small world networks increased neural communication in contrast to non-structured neural networks on flat surfaces [80].

2.2 Cell Adhesion Force Measurement

Quantifying the strength of cellular adhesion is one factor that characterizes the quality of cellular function. Comparing the produced values from a variety of experiments, and the analysis of cells under different conditions gives a better understanding on the cellular responses to changes in their environment. Since responses are often specific to cell type, the adhesion forces may be characteristic values to a certain type of cells. Several studies were able to quantify and analyze the adhesion of different types of cells either in different conditions or on different substrates.

The adhesion of a single living chondrocyte cell to a substrate was measured through AFM at three different time points of seeding. The strength of adhesion of around 30 individual cells in each condition was evaluated from the lateral detachment force over the cell area. The measured adhesion force greatly increased from an average value of 74.14 nN after 3 hours to an average value of 171.02 nN after 6 hours. After 24 hours from seeding, the cells slightly increased to an average value of 185.48 nN [81].

The initial adhesion of ligament fibroblasts on glass substrates coated with fibronectin was achieved through a micromanipulation technique. Also, the adhesion behavior to fibronectin concentrations was found to be well defined. The separation force of anterior cruciate ligament fibroblasts was found to be around 11 nN after 45 minutes from seeding on the substrate. That of the medial collateral ligament fibroblasts was 16.4 nN [82].

Another study used the AFM principle-dependent nanotweezers to measure variations in force values in cell-cell and cell-substrate interactions. The detachment force was measured for C2C12 mouse myoblast adherent cells at different contact times. The cells had an average clamping force of 43 nN and a maximum adhesion force of 47.5 nN. The cell that was completely detached was reinserted on another cell to analyze its intercellular interaction [83].

Chapter 3

Research Aims

3.1 First Aim: Study the effect of surface nano-roughness on the viability and adhesion of neuroblastoma cells and astrocytes

Hypothesis A: We will test the hypothesis that varying surface nano-roughness influences cellular viability.

Hypothesis B: We will test the hypothesis that varying surface nano-roughness influences early cellular adhesion.

Challenge: Finding the surface nano-roughness value that enables or promotes cellular viability and adhesion.

Approach: We will produce substrates of tunable surface roughness values at the nanometer level. We will culture SH-SY5Y cells and astrocytes on plasma-treated polyimide substrates, quantify their early adhesion and assess their viability.

Impact: The study of the interactions between the cells and the substrate surface gives an insight on the cell's intrinsic mechanical behavior for proliferation and allows to choose a better substrate as a neural interface. An optimal surface roughness can ameliorate the biocompatibility of the device and lengthen its lifetime for implantation.

3.2 Second Aim: Single cell adhesion force quantification of neuroblastoma cells on treated polyimide substrates

Hypothesis A: We will test the hypothesis that cells have adhesion forces that depend on the underlying surface.

Hypothesis B: We will test the hypothesis that surface nano-roughness affects cell-to-substrate adhesion.

Hypothesis C: We will test the hypothesis that single cell adhesion force increases with the increase of its cell area.

Challenge: Effectively detaching single adhered SH-SY5Y cells without prior trypsinization.

Approach: We will seed and grow SH-SY5Y cells at a low seeding density on the produced polyimide substrates and measure cell-substrate adhesion with the FluidFM BOT.

Impact: A well-defined cell adhesion force quantitatively describes cellular biomechanical behavior to a substrate for a better understanding of cellular active processes. Finding the substrate that increases cellular adhesion force allows the proper selection of material design that promotes a strong and tight contact between the cells and implantable device.

Chapter 4

Materials and Methods

4.1 Material Preparation

Samples of Kapton polyimide tape were cut and tightly attached to a clean square-shaped coverglass with dimensions of 22 mm by 22 mm. The polyimide polymer film tape has silicone as an adhesive and a total thickness of 50 μm. Surface areas for examination in material characterization and experimental work were in the central circular area of 36π mm^2. The samples were prepared by first cleaning them with 70% ethanol using Kimtech kimwipes and then drying out.

4.2 Plasma Etching Polyimide

Plasma etching is a technique frequently used in the development of semiconductors. It employs a process gas, which in this study is Oxygen, that dictates the way plasma reacts with the material of interest. The atomic Oxygen produces highly energetic and reactive species that bombard the sample surface and can subsequently react with the surface material. When parts of the surface break down to smaller volatile molecules, the vacuum system removes them in a process called dry physical etching. Since polyimide is a polymer, Oxygen abstracts Hydrogen atoms from its surface to achieve etching.

Plasma Etch PE-25 System series machine was used to etch and roughen the polyimide surface. Oxygen gas flow rate was adjusted to allow a vacuum pressure of 100-200 mTorr. A low vacuum chamber is suitable for increasing the etch rate while keeping etching uniformity from diminishing. The Radio Frequency (RF) power was kept at 100-125 W to encourage high etch rate and prevent erratic plasma formation that can cause melting or damage. RF power can increase etch rate up to a certain extent, so plasma duration can be adjusted to control the amount of etched material. Significant changes in polyimide surface nanoroughness values were observed in samples treated for more than 30 minutes. It

is important to note that the mentioned parameters are dependent on the sample size and thickness and on the gas mixture. Some polyimide samples were submerged in distilled water just after plasma etching to induce greater roughness extent, and then dried on the hotplate.

4.3 Ultraviolet-Ozone Surface Treatment

Other samples of polyimide sheets with a thickness of 12.7 μm were treated with ultraviolet-ozone to study its effect on the surface of the polyimide. The ultraviolet rays, along with the strong oxidation, decompose the organic compounds, then the active formation and decomposition of O_3 convert them into volatile molecules, which can be easily removed from the surface. The treatment results in ultraclean and uncontaminated sample surfaces within minutes. The polyimide films were treated for 15, 30 and 60 minutes in the Holmarc's UV Ozone cleaner.

4.4 Contact Angle Measurement

The contact angle of a substrate measures the wetting ability or extent of hydrophobicity of a solid surface. It is a characteristic that can be used to describe the surface energy of a solid material. Contact Angle measurements were taken using the dataphysics Contact Angle System that constitutes a simple microscope capturing a needle tip with a drop of liquid just above and perpendicular to a sample positioned on an adjustable stage. Each 5 μL drop of distilled water was placed on the sample surface at a speed of 1 $\mu L/s$, and the SCA20 software was used to accurately measure the angle of the drop edge. At least five contact angles were collected for each sample.

The acquired contact angle data were used to calculate the Critical Surface Tension (CST) of the sample of interest. CST is the tension at which the liquid completely wets the solid surface. Since only distilled water was used, the CST was determined by the sample that had a contact angle of zero. The liquid/vapor surface tension of distilled water is known to be 72 mN/m at 25°C.

Contact Angle measurements were collected for polyimide samples just after plasma etching treatment and several days after treatment to evaluate the wettability of the treated substrate over time. Other polyimide substrates were treated with the UV-ozone cleaner for different spans of time: 15, 30 and 60 minutes. One polyimide substrate without UV-cleaning served as a control substrate. The contact angle date was used to compare the effects of the two techniques on the solid surface tension.

4.5 Roughness Measurement

Stylus profilometry technique was utilized to characterize the surface roughness of polyimide. The system constitutes a diamond stylus that can move freely in one direction and a sample that is fixed to an adjustable stage. The set-up requires exact positioning of the stylus tip above the sample of interest. The stylus first carefully approaches the sample until it gets in contact with the sample and then starts tracing the sample surface and gathering information that is detected by a camera. The computer screen allows better visualization of the tip and the sample during tracing. The resultant trace curve of the moving tip determines the continuous measurement of the position and magnitude of the hills and valleys of a sample. The stylus tip tracing force is low, so this technique is non-destructive. To gather enough information about the substrate and get a good description of the roughness, several traces should be taken in different regions and directions. Different measurements require precise positioning of the sample and adjustment of the stage after each single acquisition. The resultant pre-averaged roughness values for each scan are averaged to obtain a characteristic of one sample.

The roughness of a clean polyimide sample was measured using the DekTak Stylus with a $2\mu m$ tip for better accuracy on the nanometer scale. By using the Vision 64 software, the samples can be loaded and then examined for several times and different areas. A standard scan examining the hills and valleys of the substrate with a range of 6.5 μm was employed with a tip force of 0.5 mg. Scan resolution was kept at a high value of 0.167 $\mu m/pt$ for 1000 μm measurement lengths. The filtered roughness of each measurement was obtained by a Gaussian regression with a long cutoff at 0.08 mm. At least 10 measurements in the central region of examination of the polyimide substrate were collected to evaluate the average surface roughness. Maintaining the same measurement parameters allows direct comparison of different samples.

Another technique called Digital Holographic Microscopy (DHM) measured the roughness of the conductive material graphene and captured its surface topography. The high reflectivity of the bare polyimide material did not allow it to be analyzed with the DHM. The DHM records the light wave originating from the sample as a hologram that requires a coherent light source. Both techniques measure the sample roughness without interfering with the sample and without coating it.

4.6 Surface Topography Characterization

Polyimide samples were scanned by Atomic Force Microscopy (AFM) at the Lebanese Atomic Energy Commission to construct 3D images of the plasma-

etched surface structure and acquire roughness measurement data. AFM technique includes a cantilever equipped with a probe tip that gets in contact with the sample surface. The displacements of the sharp tip are detected by a piezo scanner while maintaining a constant deflection of the cantilever.

4.7 Cell Culture

SH-SY5Y neuroblastoma cells were generously provided by Dr. Wassim Abou Kheir. Undifferentiated SH-SY5Y cells were routinely maintained on tissue culture plastic in Dulbecco's Modified Eagle Medium (DMEM) F12 Ham containing 10% Fetal Bovine Serum (FBS), 1% sodium pyruvate, 1% non-essential amino acid, 1% penicillin-streptavidin and 0.2% Plasmocin prophylactic at 37°C, 95% atmosphere and 5% CO2. The cells were usually grown and regularly maintained from a seeding density of 1.5 x 10^5 cells/mL. For cell adhesion experiments, the cells were seeded in a 6 well-plate at a density of 4.0 x 10^5 cells per well. For the FluidFM adhesion experiments, SH-SY5Y cells were seeded at a density of 2.0 x 10^5 cells per well and maintained 1-3 days before experiment. In this experiment, SH-SY5Y cells were used at day 3 and had a passage number of 28.

NHA were generously provided by Dr. Marwan El Sabban. They were maintained in Astrocyte Basal Media (ABM) supplemented with 10% Fetal Bovine Serum (FBS) and 1% penicillin-streptavidin at 37°C, 95% atmosphere and 5% CO2. For the adhesion and viability experiments, astrocytes were seeded in a 6 well-plate at a density of 2.3 x 10^4 cells per well on the regular tissue culture plastic or the polyimide substrates that were coated with Poly-L-Lysine (PLL). In both experiments, their passage number was 7.

4.8 Trypan Blue Exclusion Test for Cell Viability

Trypan Blue Exclusion assay is a simple and quick approach to measure cell viability. For this assay, cells were seeded in 6 well plates on regular well plastic, coverglass or polyimide substrate under investigation. SH-SY5Y cells were seeded at a density of 0.2 x 10^6 cells/well in the center of the well or substrate without manual distribution of the cells to prevent them from adhering outside of the central region of examination. The cells were then delicately supplemented with their complete medium. After 48 hours in culture, the cells from each well were collected and resuspended in 1 mL Phosphate-Buffered Saline (PBS) each. In an eppendorf tube, 30 μL of the cells solution were mixed with 4% Trypan Blue. From that mixture, 10 μL was added twice to the cytometer grids below a coverslip. The cells immediately spread in the chamber by capillary action. The

cytometer was mounted on a light microscope at 10X magnification to count the number of viable and non-viable cells within 5 minutes of preparing the aliquot. An intact cell membrane excludes the trypan blue dye and has a clear cytoplasm while a dead cell has a blue cytoplasm. Viability percentage was calculated as the number of viable cells versus the total number of counted cells. The cells from each well were mounted several times on the cytometer. The cells counted in the squares were averaged to find the total number of cells.

For the NHA viability test, astrocytes were seeded at a density of 2.3 x 10^4 in the middle of the well or polyimide substrate. After 5 days in culture, each of the supernatant and the trypsinized cell solution was taken separately for assessment. Trypan blue was added to each eppendorf according to its volume. On the mounted cytometer, 8 squares were counted for the supernatant, and 16 squares were taken for the trypsinized cells. Calculations of the total cell number gave the percent viability results. For the NHA viability study, two sets of experiments with similar polyimide roughness values were performed.

4.9 Initial Cell Adhesion

To study the cell adhesion on the different substrates, a 2 hour cell incubation period was taken to be the time point for initial adhesion evaluation. This period of time allows the SH-SY5Y cells to adhere to a substrate before greatly secreting their endogenous matrix proteins that can facilitate their adhesion to the substrate. Longer incubation time can become independent of the substrate sample of interest.

SH-SY5Y cells were seeded in a 6 well plate on a regular plastic surface serving as a positive control, a coverglass, or a polyimide sample with a known average roughness. Plating density was 0.4 x 10^6 cells/well. A homogeneous distribution of cells is crucial for the success of the experiment and the interpretation of data. After 2 hours from seeding, the unbound cells were collected by delicately changing the media. At least 10 random images from each well were captured by a light microscope at 20X magnification using the Zen software. The number of adhered cells was counted using an image-processing software (ImageJ, National Institutes of Health, Bethesda, MD,USA). The Analyze Cell Counter plugin tool was used to count each cell in each image.

The same method was used to determine the initial adhesion of the NHA on control well and the polyimide substrates with varying roughness values. Seeding density was at 2.3 x 10^4 cells per well or substrate. Since the experiment was performed without collecting unbound cells, the same NHA experiments were done for the viability and adhesion studies.

4.10 Scanning Electron Microscope

A Scanning Electron Microscope (SEM) employs a focused electron beam to scan the surface of a sample and construct an image. The electron beam produces a combination of signals, including back-scattered and secondary electrons to characterize the surface chemical composition and structure, respectively.

For graphene samples, several accelerating voltages were first tested to control contrast and resolution. A medium voltage of 10-15 kV was found to reduce incident electrons to better visualize the substrate surface.

4.11 Fluorescence Staining

After 72-96 hours in culture, the substrates were transferred to a new well plate and were checked under the light microscope to clearly see the attached SH-SY5Y cells. The substrates were then delicately washed twice with PBS and fixed with 4% paraformaldehyde (PFA) in PBS for 20 minutes and washed delicately with PBS. Samples were permeabilized and blocked with 3% Bovine Serum Albumin (BSA) in PBS with 0.1% Triton-X and 10% Normal Goat Serum (NGS) for 1 hour at room temperature. Primary antibodies solutions were prepared by diluting in 3% BSA-PBS. Rabbit polyclonal Anti-FAK antibody (abcam, phospho Y397, ab4803-50) was used at a dilution of 1:200. Rabbit Phospho-Paxillin antibody (Cell Signaling, Tyr118 2541) was used at a dilution of 1:100. Each of two same set of conditions were incubated with one of the primary bodies overnight at 4°C in a humidfied chamber. The samples were then washed 2-3 times with 1X wash buffer. The secondary goat anti-rabbit antibody (Alexa Fluor 568) was diluted at 1:100 and combined with phalloidin (Alexa Fluor 488 Thermo Fisher, invitrogen A12379) and incubated for 30 minutes at room temperature. The samples were transferred to a glass slide with the addition of a mounting medium with 4,6-diamidino-2-phenylindole (DAPI). The substrates were mounted on a microscope slide and observed on a confocal microscope.

4.12 InkJet Printing

The Dimatix materials printer was loaded with PEDOT:PSS or graphene solution to print several areas of a coverslip. The solution was composed of a graphene/PEDOT:PSS hybrid ink dispersed in dimethylformamide (DMF) from Sigma-Aldrich (SKU 900442). Printing design was achieved through a bitmap file with a DPI of 2540 that contained twelve 500 micrometer squares. After printing, the PEDOT substrate was heated on the hot plate at 90°C for 3 hours, and the graphene substrate at 100°C for 1 hour.

4.13 FluidFM

FluidFM is a BOT system based on the technology of the AFM microchanneled cantilevers and specially manufactured by Cytosurge (Glattburgg, Switzerland). It consists of a hollow cantilever connected to a pressure controller through a fluid circuit. A laser detection system establishes a force feedback to monitor the contact of the probe with the loaded surface. Imaging is achieved through an inverted optical microscope (Zeiss Axio Observer.Z1, Carl Zeiss AG, Oberkochen, Germany), and the experimental preparation and parameters are controlled with the ARYA software.

4.13.1 Spotting

Nanolithography experiments were performed by the FluidFM system situated on a vibration-free table. The probes holding the cantilever can be nanopipettes or micropipettes depending on their aperture size dimensions. These can be filled with an ink solution that should be passed through a 0.2 μm filter, and an applied pressure ejects the solution from the cantilever tip. In our experiments, a micropipette with an aperture of 2 or 8 μm and a spring constant of 2 N/m was filled with 1 μL PEDOT solution and then loaded into the setup. A microscope slide of the desired substrate was inserted in its designated position on the XY-stage. A variety of pressure and duration combinations were tested to print spots at the nanometer range.

4.13.2 Single Cell Adhesion Force Measurement

After 72 hours in culture, the 6-well plate consisting of wells with a working volume of 2 mL was loaded into the BOT system encompassing an incubator that kept it at 37 °C. A micropipette with an 8 μm aperture and a spring constant of 2 N/m was filled with 1 μL of a buffer solution or 50% glycerol for storing it for further experiments. The probe was mounted to the probe holder plate firstly without the addition of the cleaning plate. After gripping the probe, positioning the laser, measuring the spring constant and preparing the system, the probe cantilever can now be used for the adhesion experiment. After taking the probe to the well with the cultured cells and aligning it, the cleaning 12-well plate can be added adjacent to the 6-well plate. This plate contained 5% sodium hypochlorite bleach solution, ultrapure distilled water and cell-free media solution filled in a number of wells. The probe can be cleaned from cell debris after each measurement through a customizable cleaning process according to pressure and time. The cantilever should be dipped in the detergent for only a few seconds and then must be rinsed several times in different wells with ultra pure water and media to remove any remaining residue for it not to reach the cells. The optimal parameters for detaching the SH-SY5Y cells were: set-point

25 mV, pressure -200 mbar and pause of 5 seconds. Those same parameters were used for the measurements taken of all the selected SH-SY5Y cells in control and polyimide samples. The retraction distance was kept at 50 μm. The resultant Force-Distance curves and relevant images were exported from the software.

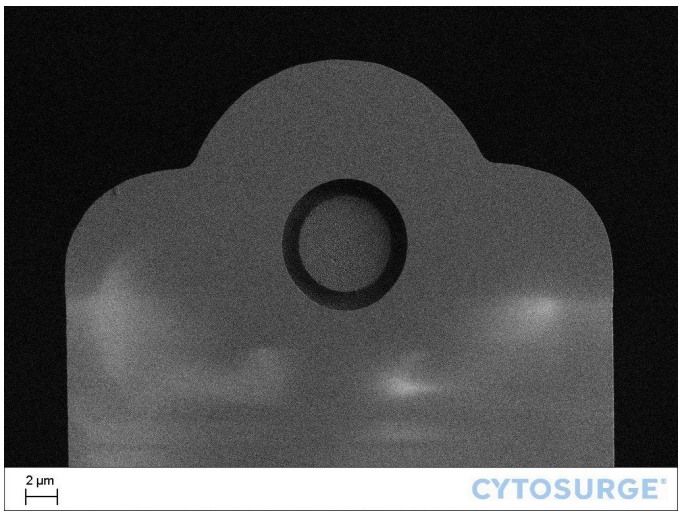

Figure 4.1: **Microscope Image of the Micropipette Used in the Adhesion Experiment.** It had an aperture of 8 μm and a spring constant of 2 N/m.

Chapter 5

Results

5.1 Contact Angle Measurement of Polyimide Substrates

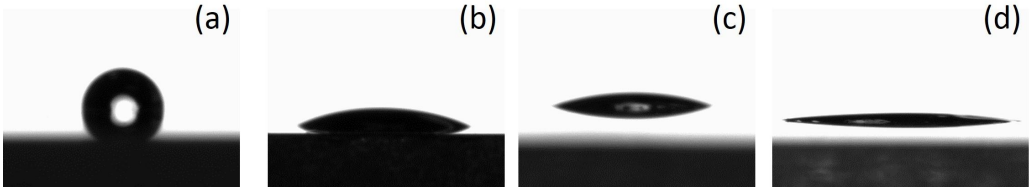

Figure 5.1: **Contact Angle Drop Images of Plasma Treated Polyimide Substrates at 85W Power.** (a) Control polyimide sample with drop angle of 100.86°. (b) Polyimide sample treated for 30 seconds with drop angle of 33.40°. (c) Polyimide sample treated for 1 minute with drop angle of 12.85°. (d) Polyimide sample treated for 2 minutes with drop angle of 9.17°.

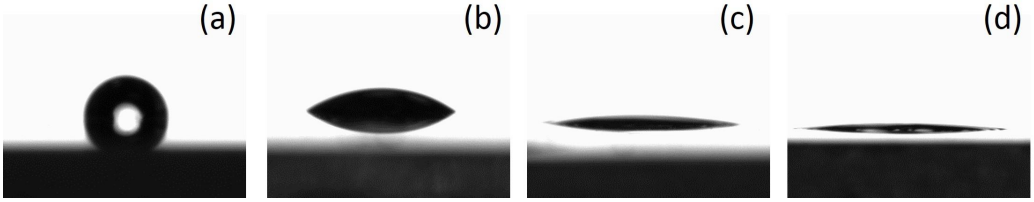

Figure 5.2: **Contact Angle Drop Images of Plasma Treated Polyimide Substrates at 150W Power.** (a) Control polyimide sample with drop angle of 100.86°. (b) Polyimide sample treated for 30 seconds with drop angle of 25.28°. (c) Polyimide sample treated for 1 minute with drop angle of 10.35°. (d) Polyimide sample treated for 2 minutes with drop angle of 7.43°.

The contact angle of polyimide substrates right after plasma treatment at powers of 85 W and 150 W had decreasing values with the extension of plasma duration. While control polyimide samples that were not treated with plasma had average contact angle of 102.26°, the contact angle of the samples treated for 30 seconds drastically decreased to values of 24.96° at 85 W and 30.42° for 150 W. The contact angle further decreased in substrates treated for 2 minutes to become 12.72° at 85 W and 7.57° at 150 W. The contact angle became negligible on substrates treated for 5 minutes in both power modes. The contact angle images are shown in Figure 5.1 and Figure 5.2. The contact angle graph of the averaged values are shown in Figure 5.3. These results were similar to the contact angle measurements of the oxygen plasma treated kapton films in [84]. The individual measurements of each substrate are included in the supplementary.

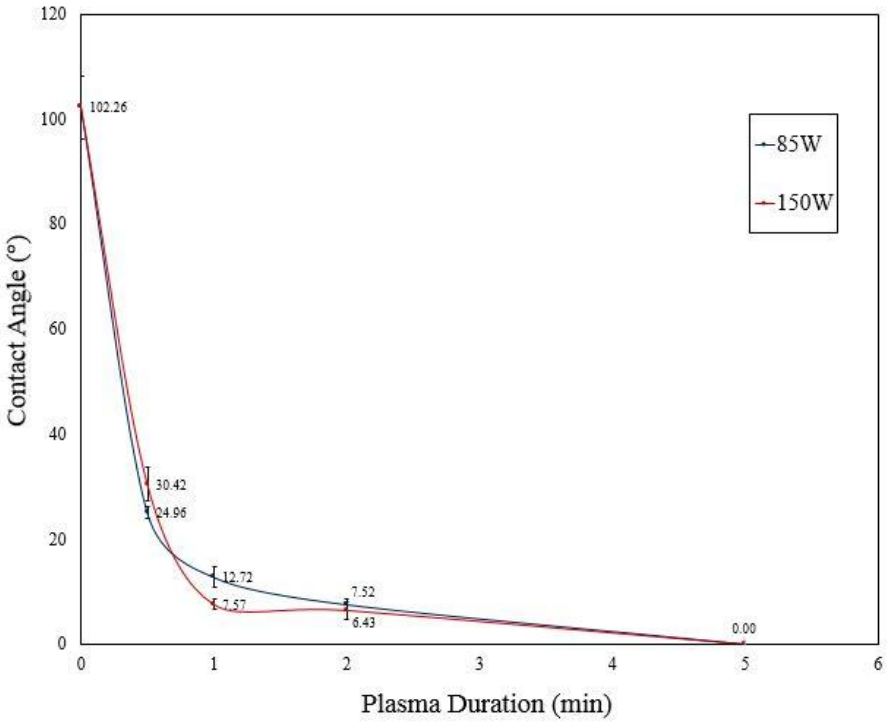

Figure 5.3: **Contact Angle Measurements of Plasma Treated Polyimide Substrates at 85W and 150W Power.**

The same polyimide substrates were measured again after 5 days from treatment. The contact angle greatly increased for all the substrates, where the contact angle of the the polyimide substrate that was treated for 5 minutes increased from 0° to 50.10°. The averaged contact angle values are plotted in Figure 5.4.

These results confirm that the plasma treatment loses its effect on the wettability of the surface over time.

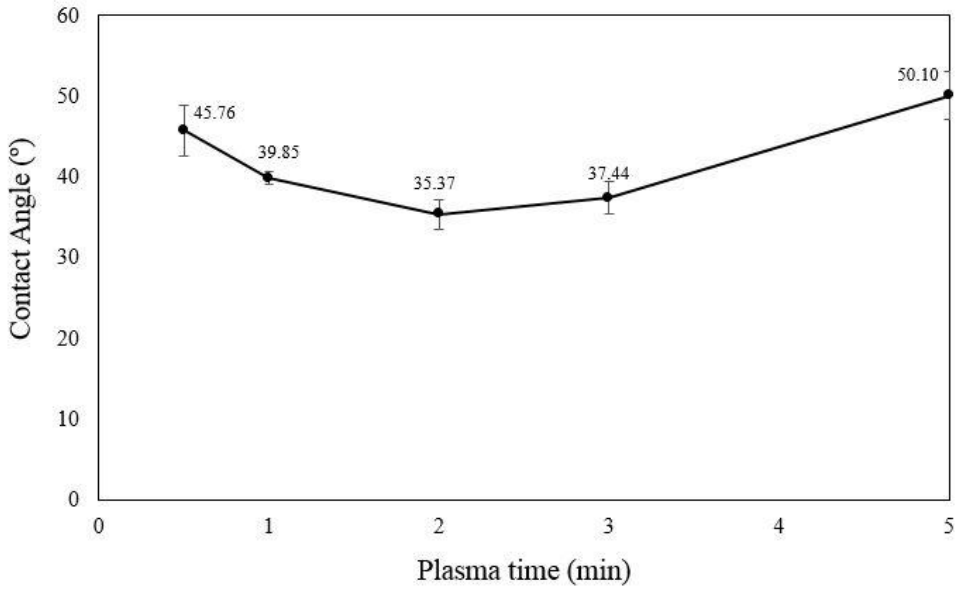

Figure 5.4: **Contact Angle Measurements of Plasma Treated Polyimide Substrates after 5 Days from Etching**

The plasma treatment effect on the contact angle was compared to that of the ultraviolet-ozone cleaning method. The contact angle of the polyimide substrate cleaned for 60 minutes reached an average value of 17.30°. The contact angle images are shown in Figure 5.5. The contact angle graph of the averaged values are shown in Figure 5.6.

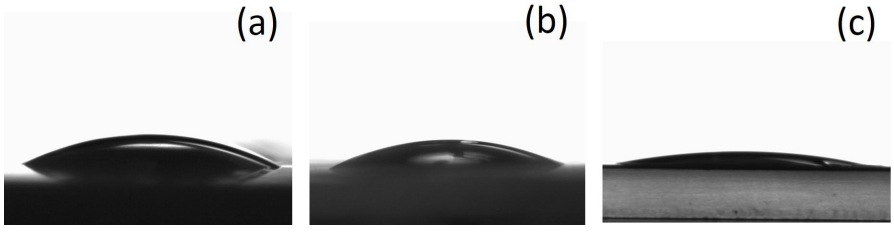

Figure 5.5: **Contact Angle Drop Images of Polyimide Samples Treated with Ultraviolet-Ozone for (a) 15, (b) 30 and (c) 60 minutes.**

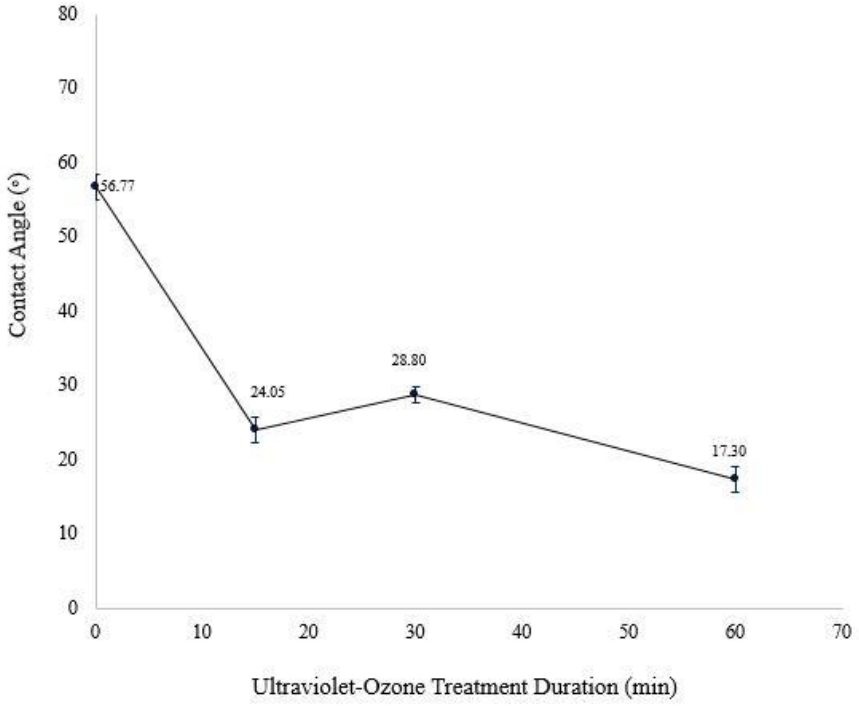

Figure 5.6: **Contact Angle Measurements of Ultraviolet-Ozone Treated Polyimide Substrates for 0, 15, 30 and 60 minutes.**

5.2 Surface Roughness Measurements of Plasma-Etched Polyimide

Polyimide samples were treated with oxygen plasma at different duration periods, vacuum pressure and RF power values. Manipulating these values produced samples with a variety of surface roughness. The graph of the average roughness (R_a) of the plasma-etched polyimide samples at 80 mTorr is represented in Figure 5.7. The lowest vacuum pressure achieved at 80 mTorr produced the surfaces with the highest R_a attained in lowest time. R_a value of 14.39 nm was achieved after only 15 minutes of etching. R_a increased with the increase in plasma duration. It slowly increased from its control value of 1.12 nm to 1.41, 1.49 and 1.94 nm after 30 seconds, 1 minute and 2 minutes respectively. A drastic increase in roughness value was observed from a value of 3.98 nm after 3 minutes to a value of 9.18 nm after 5 minutes. R_a then slightly increased to 10.36 nm at 7 minutes time point and to 11.60 nm at 10 minutes.

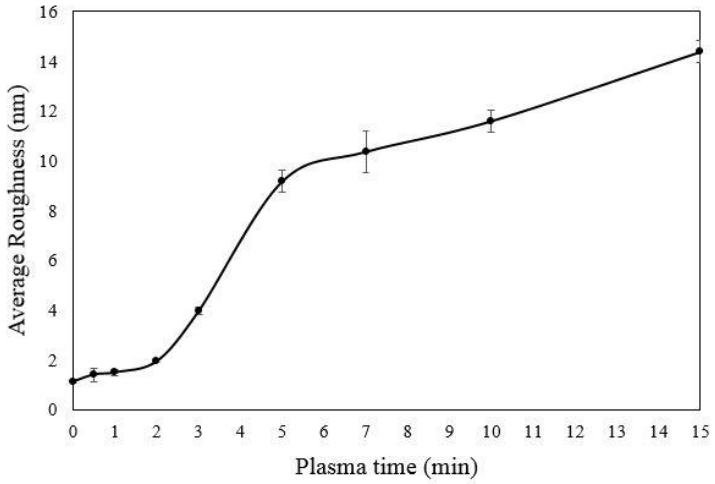

Figure 5.7: **Average Roughness of Plasma-Etched Polyimide at 80 mTorr Vacuum Pressure and 150W RF Power.**

At a higher vacuum pressure of 100 mTorr, the plasma-etched polyimide reached R_a value above 20 nm after 45 minutes. Even so, it reached a value of 7.67 nm after 1 minutes as seen in Figure 5.8, which is significantly less than the 11.60 average value reached at 80 mTorr.

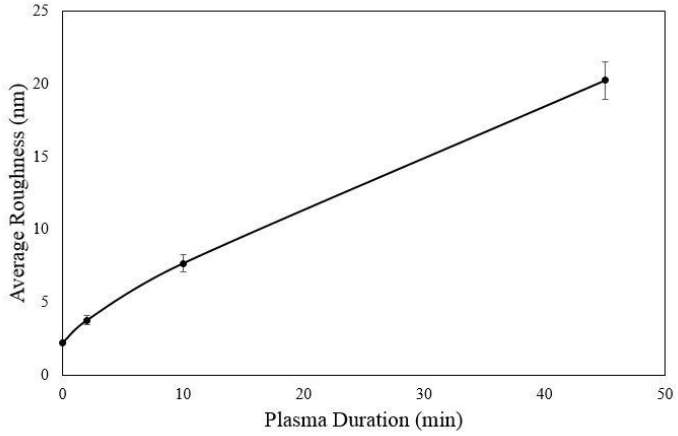

Figure 5.8: **Average Roughness of Plasma-Etched Polyimide at 100 mTorr Vacuum Pressure and 150W RF Power.**

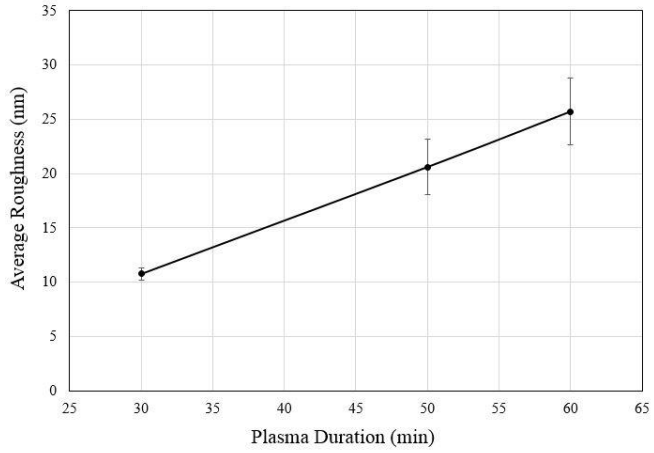

Figure 5.9: **Average Roughness of Plasma-Etched Polyimide at 200 mTorr Vacuum Pressure and 150W RF Power.**

When increasing the plasma duration and RF power, the surface roughness loses part of its homogeneity and becomes more variant along the same surface. In Figure 5.9, roughness values of plasma-etched polyimide samples for 50 and 60 minutes at 150W had high error values.

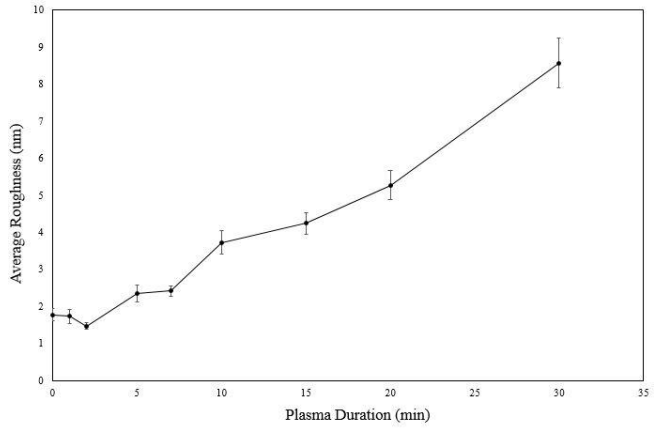

Figure 5.10: **Average Roughness of Plasma-Etched Polyimide at 200 mTorr Vacuum Pressure and 100W RF Power**

At 200 mTorr vacuum and 100W power, polyimide sample etched for 30 minutes could not achieve R_a greater than 10 nm only. It increased from 3.73 nm after 10 minutes, to 4.25 nm after 15 minutes and 5.28 nm after 20 minutes until it reached 8.57 nm at 30 minutes. (Figure 5.10)

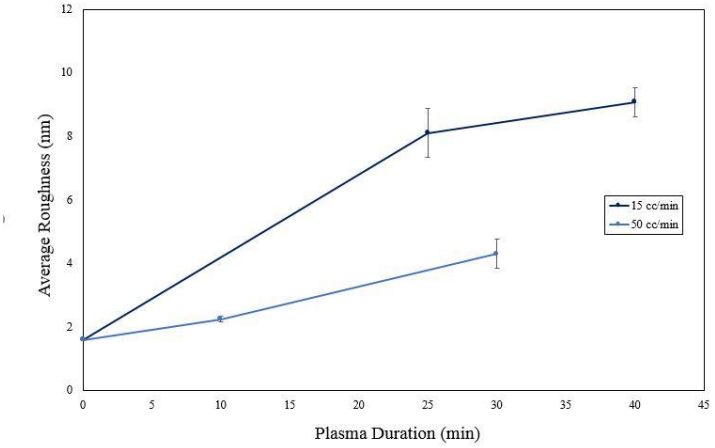

Figure 5.11: **Average Roughness of Plasma-Etched Polyimide at 15 and 50 cc/min Air Flow at 100W RF Power.**

The polyimide roughness increase at a gas flow rate of 50 cc/min which corresponds to maximal vacuum pressure was slower than that of 15 cc/min which establishes a vacuum pressure of 200 mTorr, as demonstrated in Figure 5.11. After 30 minutes etching at high vacuum pressure, R_a only reached 4.31 nm. On the other hand, after 25 minutes etching at 200 mTorr, the polyimide substrate already achieved 8.11 nm roughness value.

The trend in the increase of average roughness with the increase in plasma duration was similar in two separate runs of polyimide samples at the same vacuum pressure. Figure 5.12 describes the reproducibility of R_a in polyimide samples.

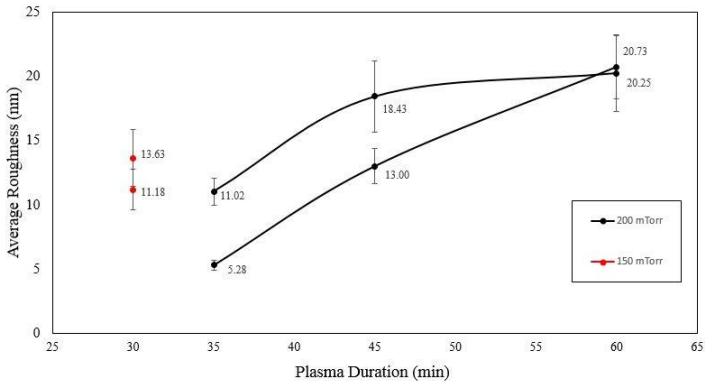

Figure 5.12: **Reproducibility of Polyimide Substrates.** Average roughness measurements from 2 runs at the same parameters at 125 W.

5.3 Polyimide Surface Topography Characterization

AFM was used to characterize the three dimensional topography of the plasma-etched polyimide substrate for a better visualization of its geometrical features. As seen in Figure 5.12, the polyimide substrate etched for 15 minutes had relatively short hills on its surface with some areas still retaining their flat feature. The sample etched for 30 minutes had a much more roughened surface with hill structures reaching height values above 50 nm.

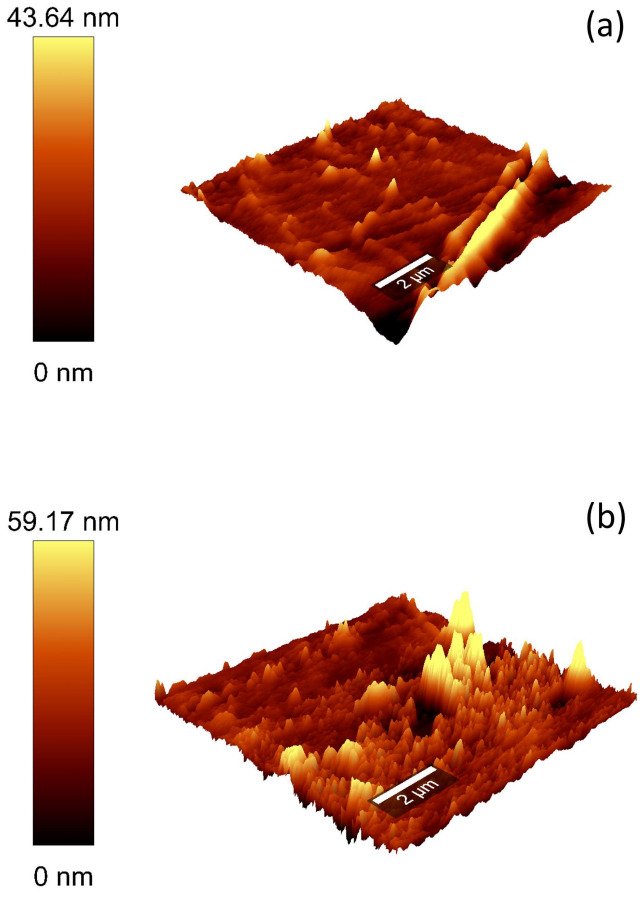

Figure 5.13: **AFM 3D topographical images of Polyimide substrates plasma-treated** for (a) 15 minutes and (b) 30 minutes. Scale bar: 2 μm.

5.4 Roughness Measurement of Graphene and PEDOT:PSS

The surface nano-roughness values were measured and compared in spin-coated Graphene/PEDOT:PSS coverglass, InkJet-printed Graphene/PEDOT:PSS and InkJet-printed PEDOT:PSS. The spin-coated graphene provided surface roughness values in the low nanometer range. It also provided good optical transparency that could be achieved by coating a thin homogeneous layer of graphene. Spin-coating graphene is a simple method for producing different surfaces at the low nanometer roughness range, without the need of sophisticated methods. Graphene gives the surface randomly shaped structures while PEDOT:PSS exhibit smaller features with smooth outlines as seen in Figure 5.14.

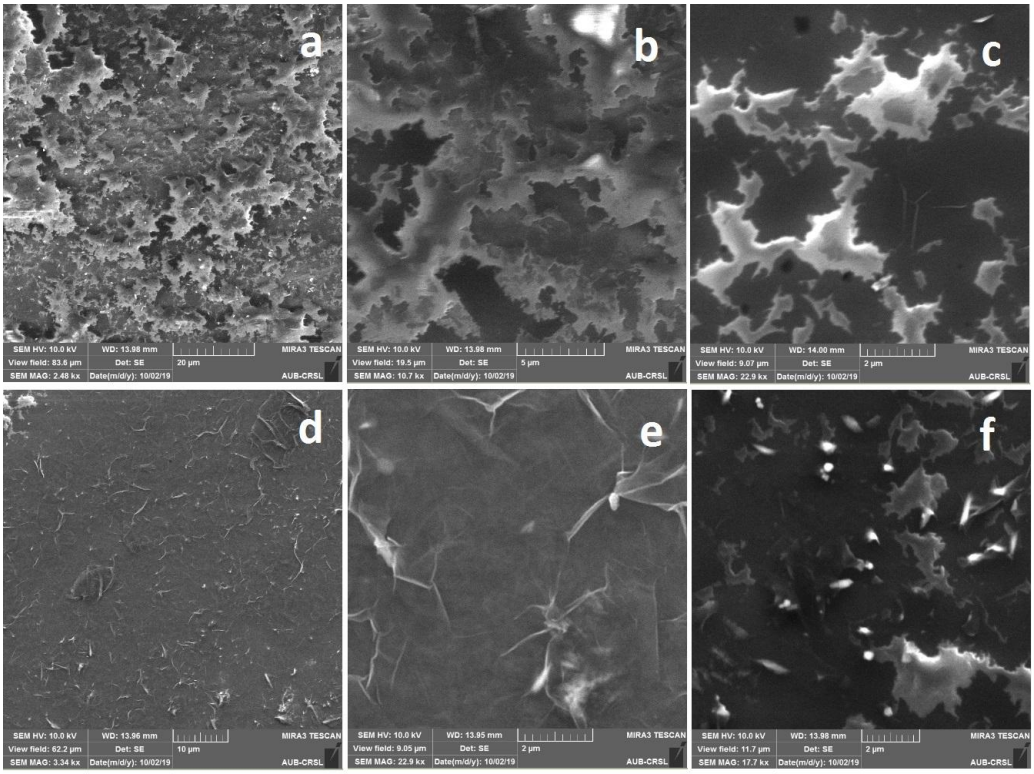

Figure 5.14: **SEM micrographs of graphene solution spin-coated on a glass slide.** Cured graphene formed flaky structures. (a) Scale bar: 20 μm (b) Scale bar: 5 μm (c) Scale bar: 2 μm (d) Concentrated PEDOT particles Scale bar: 10 μm (e) Scale bar: 2 μm (f) Graphene flakes surrounded by PEDOT particles. Scale bar: 2 μm.

Spin-coated graphene surface roughness measurements and profiles were at low nanometer values in Figure 5.15. In addition, the topographical plot of the spin-coated graphene indicates the appearance of a few hill structures with small heights, which were quantified in Figure 5.16.

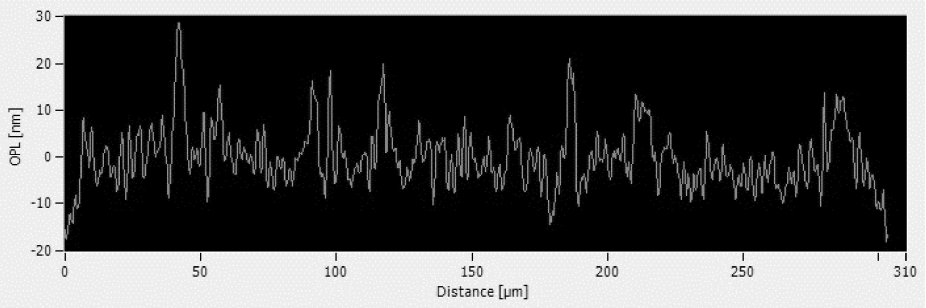

Figure 5.15: **Surface profile of a graphene substrate** along the diagonal of the area with the 8.14 nm roughness.

Graphene/PEDOT:PSS and PEDOT:PSS were both InkJet printed with the same selected spots size and position. The InkJet printing of graphene at 45°C yielded an improved consistency of the printed material as opposed to the PEDOT printed at 30°C. The micrographs of the printed graphene squares are shown in Figure 5.17. The graphene squares were not evenly printed with high accuracy; however, they were still able to produce average roughness values that are similar. For the measurements, each printed square was sectioned into 5 regions to see the difference of roughness values across the square area. In graphene, the roughness values from each section were not highly variant, as shown in Figure 5.18. On the other hand, the PEDOT squares were heterogeneously printed, as seen in Figure 5.19. The roughness measurements along the length of each section were highly variant, and the averaged roughness of each square had very high standard deviation values. It was even difficult to compare the surface roughness values of different squares. The results of the surface roughness measurements from the DekTak profiler are in Table 4.1.

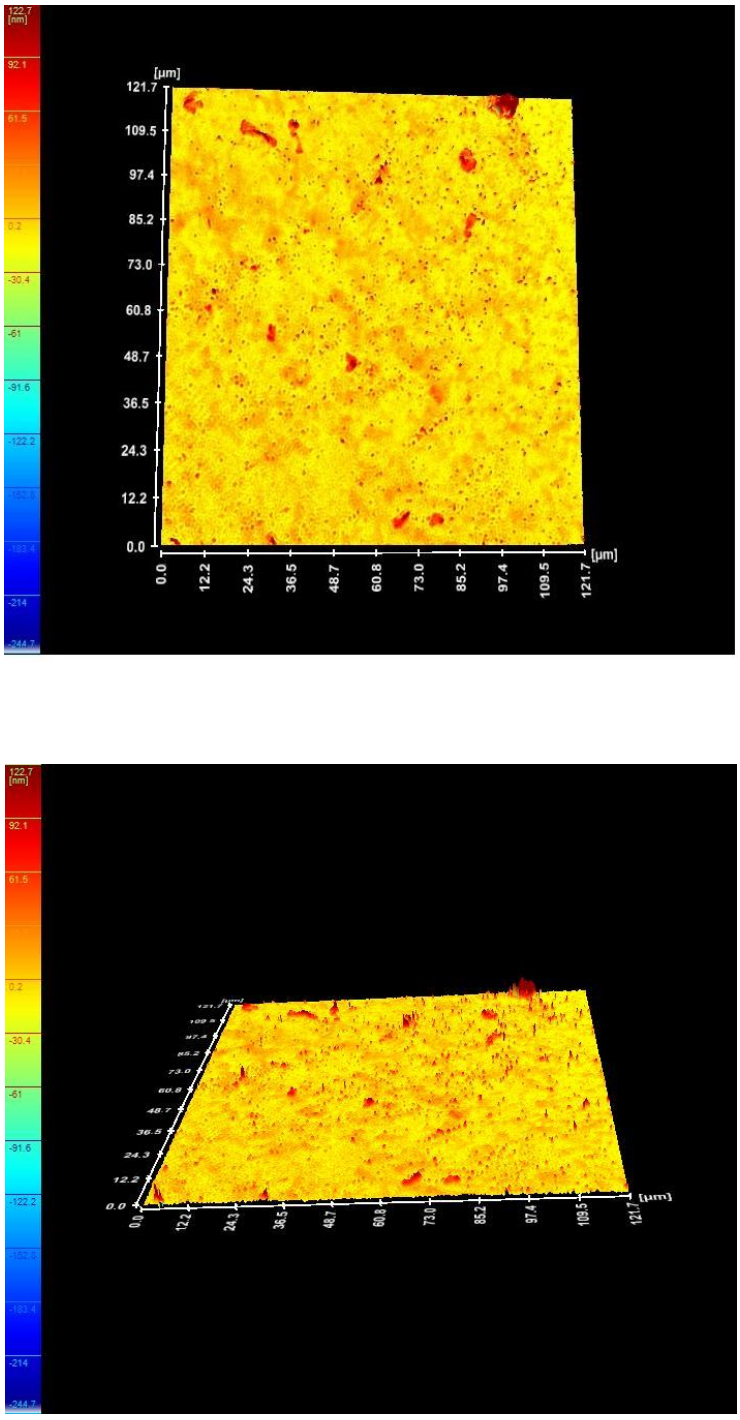

Figure 5.16: **DHM 3D perspective plots of a graphene substrate.** The two DHM plots correspond to the same area of a spin-coated graphene substrate with a roughness value averaging at 8.14 nm.

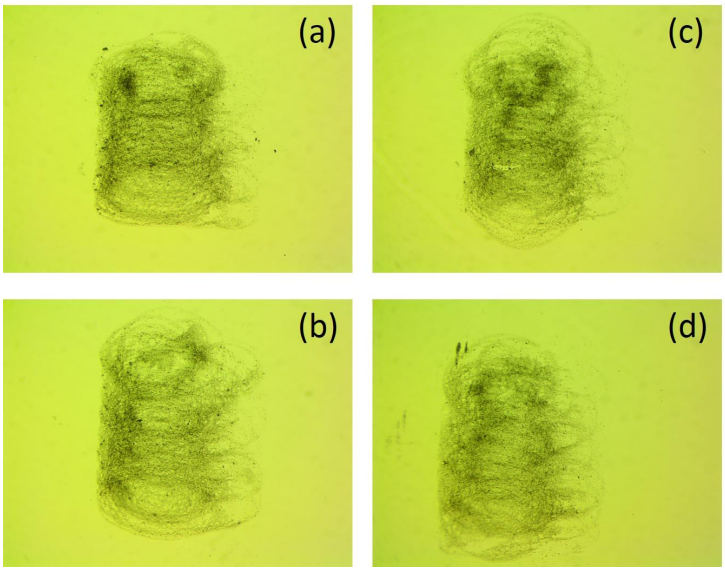

Figure 5.17: **Micrographs of InkJet-Printed Graphene Squares** (a) 1 (b) 2 (c) 7 and (d) 8 .

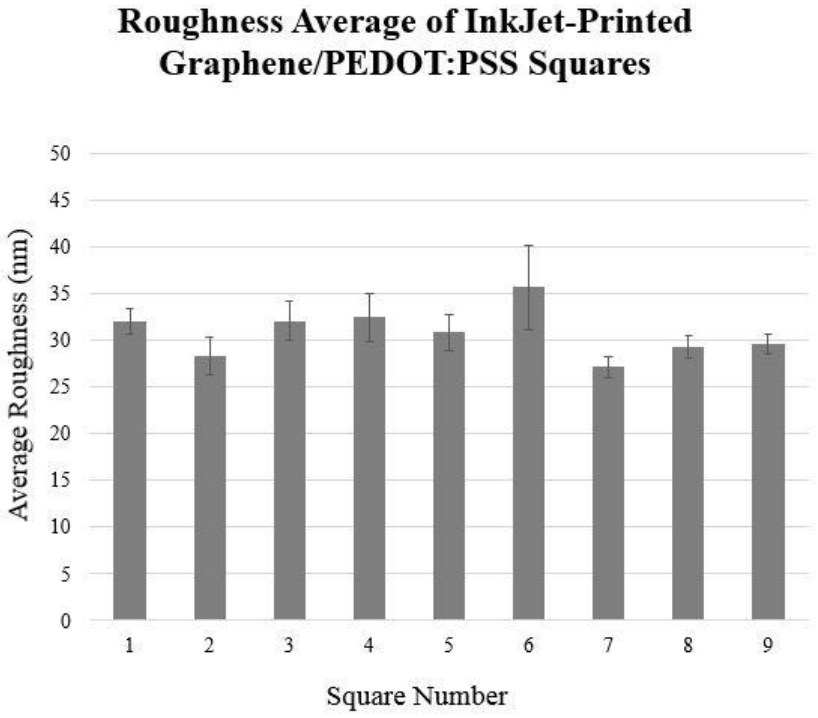

Figure 5.18: **Average Roughness of InkJet-Printed Graphene Squares.**

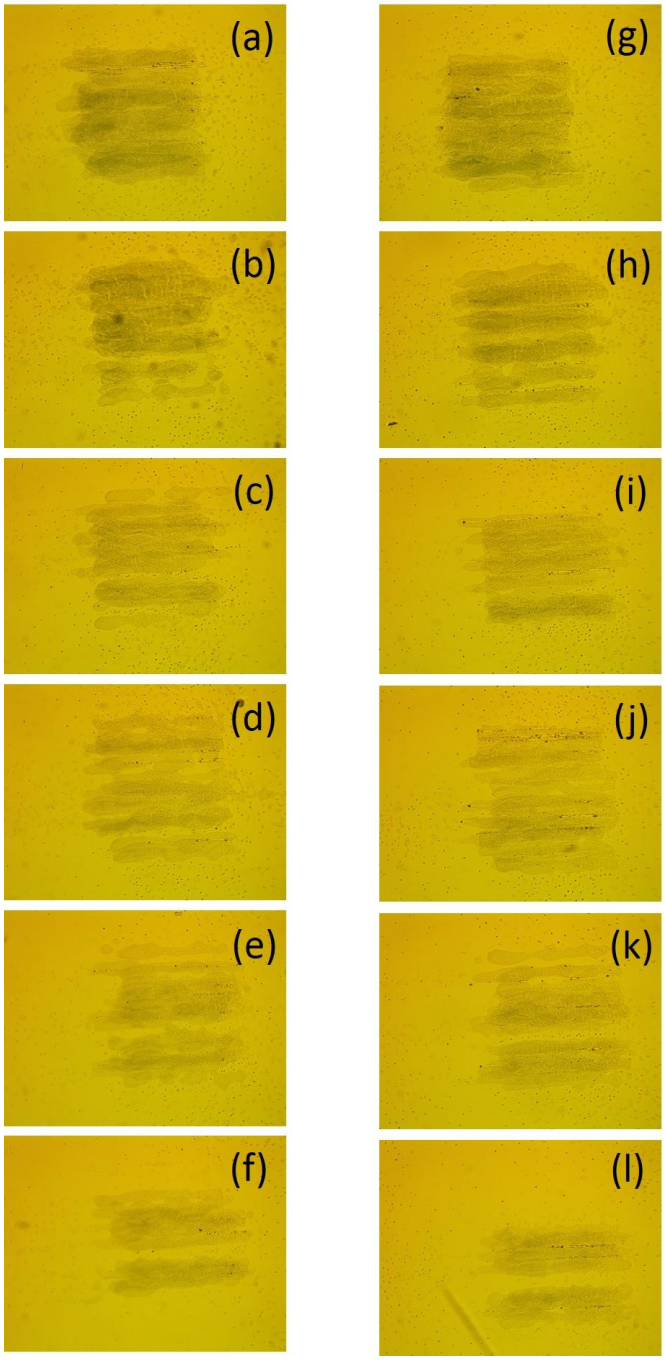

Figure 5.19: **Micrographs of Each InkJet Printed PEDOT Square** The two columns of images are represented in the same way that they were printed on the coverglass.

	Measurement Number						
PEDOT Square	**1 (nm)**	**2 (nm)**	**3 (nm)**	**4 (nm)**	**5 (nm)**	**Average (nm)**	**Standard Deviation (nm)**
Glass	7.55	8.36	2.92	5.35	4.56	**5.75**	2.21
(a)	50.44	23.38	22.03	83.05	36.66	**43.11**	25.12
(b)	49.9	64.7	71.64	49.07	18.98	**50.86**	20.27
(c)	65.77	27.75	36.62	19.8	28.58	**35.70**	17.83
(d)	21.04	32.93	28.39	29.83	24.45	**27.33**	4.65
(e)	22.46	39.35	38.04	35.72	32.75	**33.66**	6.75
(f)	22.56	19.99	69.41	30.62	35.17	**35.55**	19.89
(g)	55.82	46.87	56.05	33.15	81.75	**54.73**	17.75
(h)	34.08	56.84	14.52	31.18	79.23	**43.17**	25.17
(i)	49.35	27.13	76.14	28.72	22.59	**40.79**	22.28
(j)	19.61	81.19	30.85	51.29	31.53	**42.89**	24.26
(k)	21.91	40.18	55.88	16.64	39.39	**34.80**	15.73
(l)	19.85	31.86	56.6	38.39	10.43	**31.43**	17.73

Table 5.1: **Roughness values for each square of Inkjet printed PEDOT:PSS.** Each drop was measured for 5 times using the Gaussian option on the Vision 64 software. Dots were varied in roughness and did not have homogeneous surfaces. Drop name corresponds to the number of its column followed by its position along that column. Coverglass roughness measurements adjacent to the printed squares were taken as a reference. Each square was sectioned into five sections, so the measurement numbered 3 takes the roughness value along the middle region of the square.

5.5 Cell Viability

After 48 hours in culture, the SH-SY5Y cells adhered on the control polystyrene tissue culture plastic, coverglass and polyimide substrates with varying nanometer roughness values were collected. The experiment was performed twice, and the averaged viability percentages are displayed in the graph of Figure 5.20. In the control well, 88.3% of the cells were viable. The well with the coverglass had a 86.2% of the cells viable but with most of them being detached from its surface. All other substrates had minimal floating cells and cells growing outside substrate border. Very smooth polyimide substrates allowed the viability of 90.4% of SH-SY5Y cells. Polyimide substrates with a 4.1 nm average surface roughness resulted in 86.5% viability. Substrates of 8.1 and 12.1 average roughness both achieved 93.2% and 93.5% viability percentages respectively. One substrate with $R_a = 25.9$ nm yielded 90.8% viability of SH-SY5Y cells. The plot in Figure 5.20

corresponds to the average of cells of two passage numbers: 28 and 29.

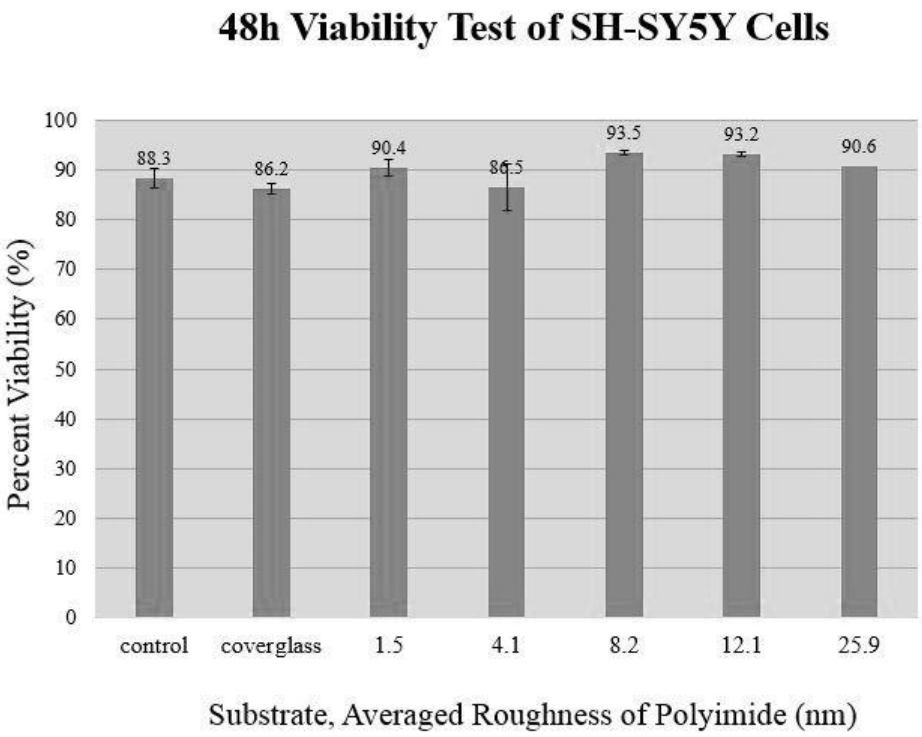

Figure 5.20: **Percent Viability of SH-SY5Y Cells vs. Polyimide Average Roughness**

5.6 Initial Adhesion of SH-SY5Y Cells

The cell-substrate adhesion was evaluated after 2 hours from seeding. The number of adhered SH-SY5Y cells was determined from several microscope images through ImageJ analysis. The resultant counts were normalized with respect to the control and averaged from several trials. When evaluating the trials, the results from substrates with similar R_a values were grouped together. In this case, substrates with R_a values of 2.62 and 8.5 nm were from five trials, and substrates with R_a values of 12.68 and 6.68 nm were from three trials. The cells from the trials with passage numbers from 22 to 25 were seen to follow a common trend. SH-SY5Y cells attained 82.51% adhesion on the smooth polyimide substrates with R_a = 2.62 nm. They were able to attain an average adhesion percentage of 213.77% on R_a = 8.05 nm, 102.3% on R_a= 12.68 nm and 90.17% on R_a = 16.68 nm. Meanwhile, only 26% adhered to the coverglass substrate.

The percent adhesion was therefore maximal around surface nanoroughness value of 8 nm. The graph is represented in Figure 5.22. The adhesion percentage had very high values for the calculated standard error from the different trials.

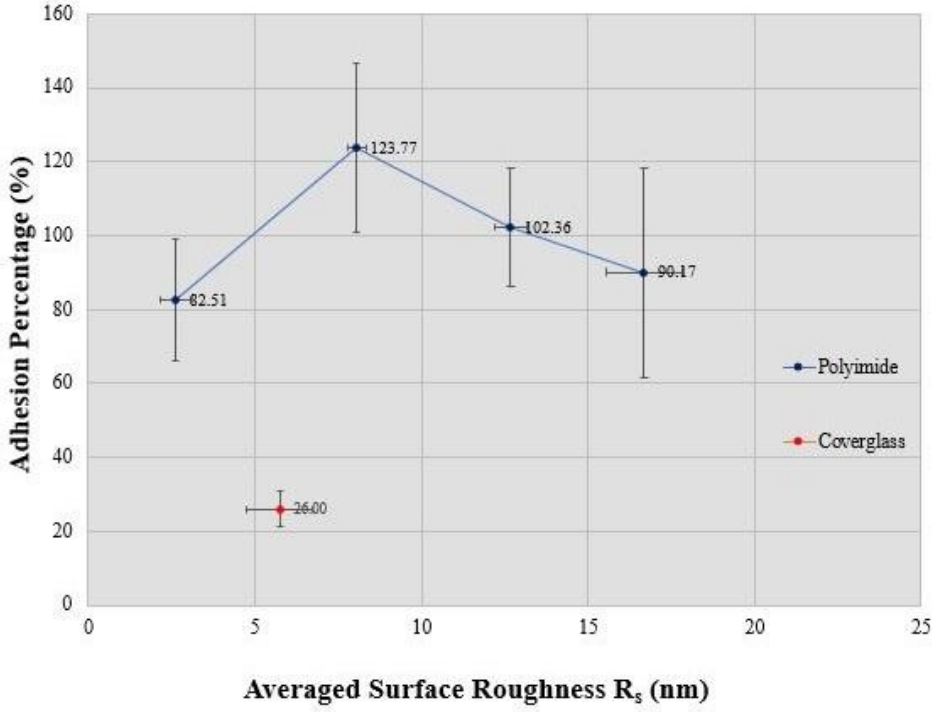

Figure 5.21: **Percent Adhesion of SH-SY5Y Cells on Nano-Rough Polyimide Substrates** Passage number 22-25.

In four other trials, the cells with passage numbers from 34 to 36 were seen to follow a trend different from the cells with lower passage numbers. In this case, the polyimide substrates used in each trial had very similar average roughness values, so each percent average calculated corresponds to the average of four trials of each substrate. SH-SY5Y cells attained 120.331% average percent adhesion on the smooth polyimide substrates with $R_a = 1.68$ nm. They attained 116.07% on $R_a = 4.84$ nm, 99.83% on $R_a = 11.05$ nm and 105.33% on $R_a = 20.7$ nm. In addition, 127.22% adhered to the coverglass substrate. The relevant graph is represented in Figure 5.23.

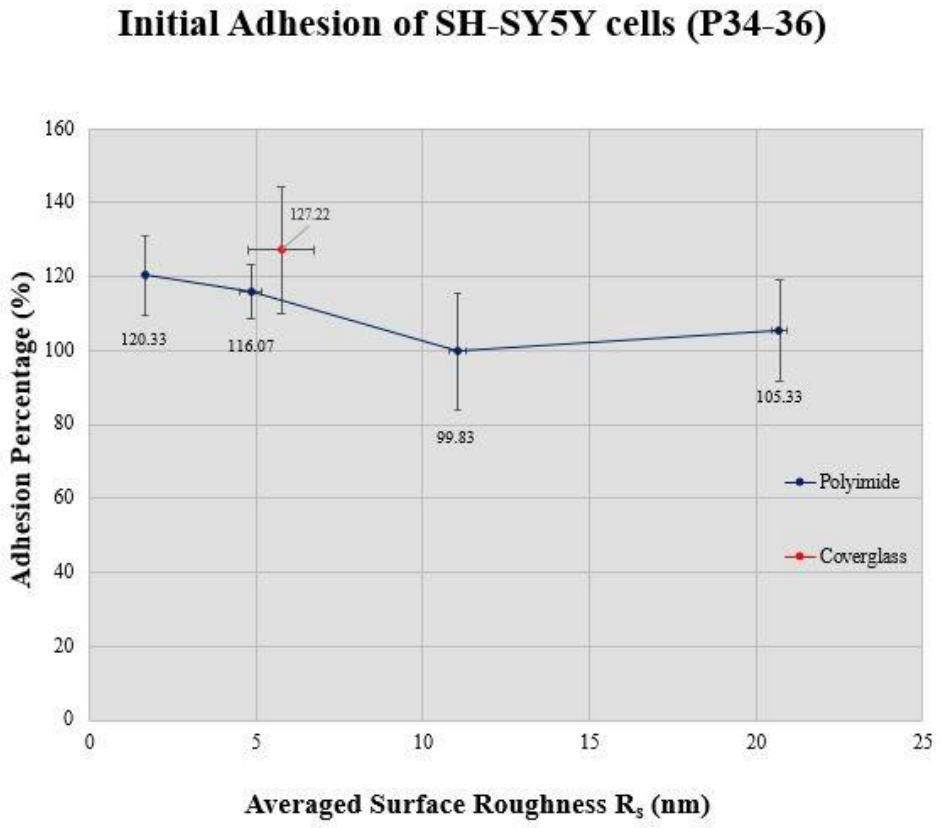

Figure 5.22: **Percent Adhesion of SH-SY5Y Cells on Nano-Rough Polyimide Substrates.** Passage number 34-36.

After 3 days in culture, SH-SY5Y cells were fixed and immunostained to quantify the expression of FAK and paxillin. Figures 5.23 and 5.24 represent the control samples for FAK and paxillin, respectively.

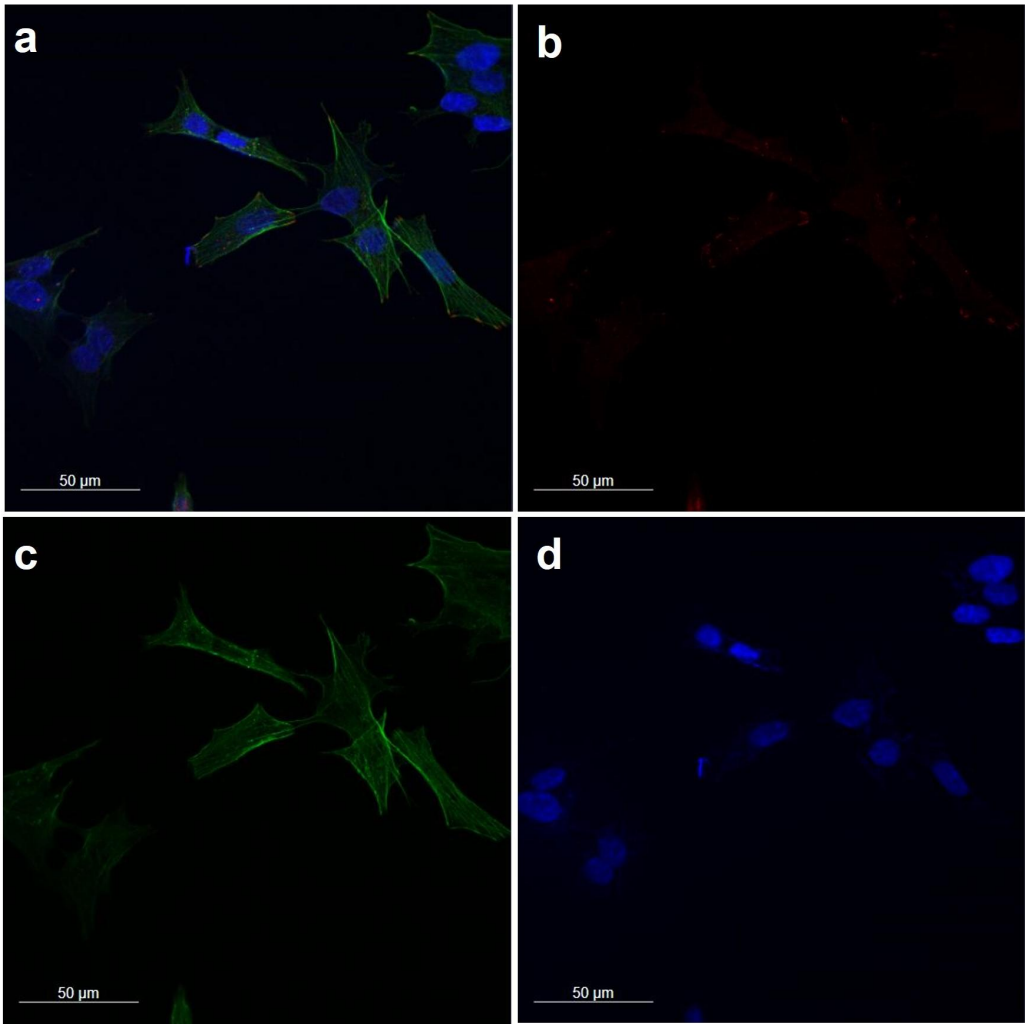

Figure 5.23: **Confocal Microscopy Images of SH-SY5Y Cells on Coverglass.** SH-SY5Y cells were immunostained with (b) Focal Adhesion Kinase. (c) Phalloidin and (d) DAPI were used to visualize the F-actin and nucleus respectively.

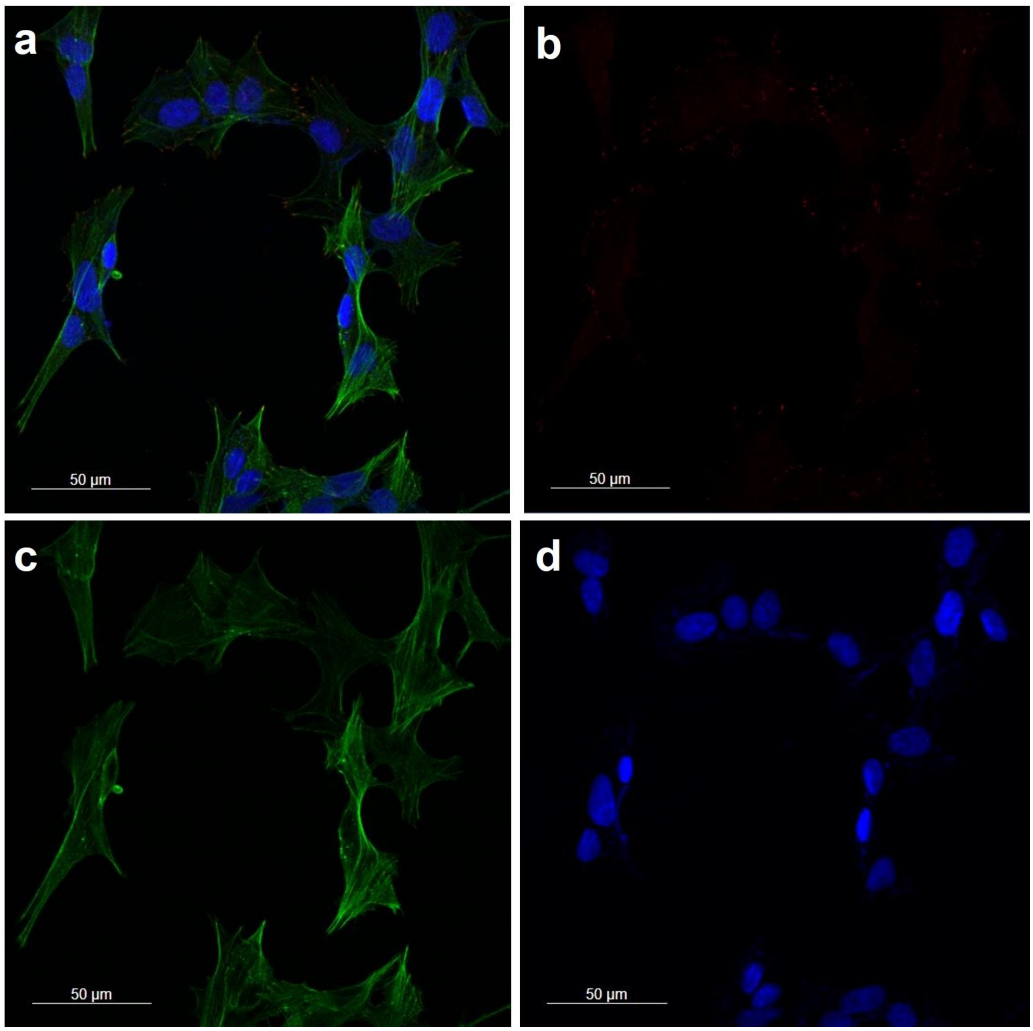

Figure 5.24: **Confocal Microscopy Images of SH-SY5Y Cells on Coverglass** SH-SY5Y cells were immunostained with (b) phospho-paxillin. (c) Phalloidin and (d) DAPI were used to visualize the F-actin and nucleus respectively.

The cell viability test was performed twice for the NHA at day 5 in culture. The astrocytes successfully adhered and proliferated on the control and polyimide substrates. The percent viability of the NHA adhered to the polyimide substrates with varying surface nanoroughness values were normalized to the average of the percent viability of the control samples. Figure 5.25 represents the linear correlation between the percent viability and the average surface roughness values. The graph shows a trendline that is relatively horizontal, which indicates that the percent viability was not significantly varying across the variations in surface roughness values. The highest percent viability of 111.37% that of control was

for the polyimide substrate with a 9.7 nm average roughness value. The lowest percent viability of 89.59% that of control was for the polyimide substrate with a 6.62 nm average roughness value.

After 2 hours from seeding, the NHA were imaged and counted to produce the graph in Figure 5.26. The number of initially adhered NHA on control samples were higher than most of the polyimide substrates. The highest cell count was for the polyimide substrate with an average roughness of 3.98 nm followed by that of 9.71 nm. The lowest cell count was that of the substrate with a 14.38 nm average roughness.

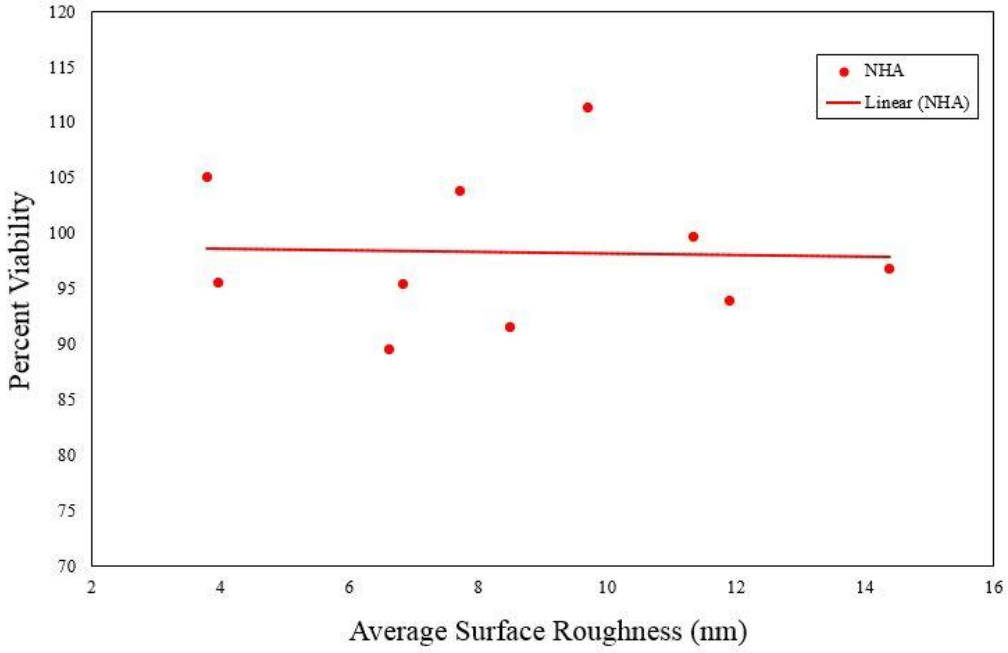

Figure 5.25: **Percent Viability of Normal Human Astrocytes on Polyimide Substrates With Varying Average Roughness Values.**

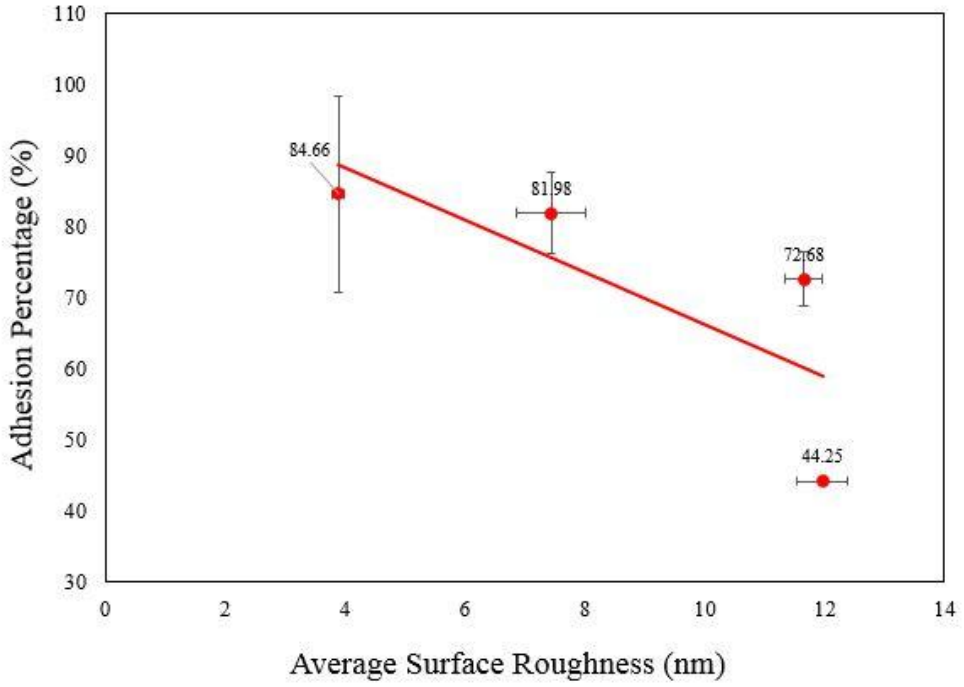

Figure 5.26: **Initial Adhesion of NHA on Polyimide Substrates With Varying Average Roughness Values.**

5.7 Single Cell-Substrate Adhesion Force

The detachment forces of single adhered SH-SY5Y cells on regular polystyrene and roughened polyimde substrates were measured through the FluidFM robotic system. The resultant force-distance curve is represented in Figure 5.27. The force curve initiates from a point of no contact between the cantilever and the cell. The cantilever first establishes a contact with the cell to ensure it's well gripped to the cantilever aperture. As the cantilever moves upward, it exhibits negative forces. As it moves further, the cell undergoes deformation until fully detached from the surface. During retraction, the tip reverts to its original state before bending in a slow movement.

Since the SH-SY5Y cells were seeded at low confluency, the resultant measured force represents the substrate adhesion strength of the single whole cell. From the graph in Figure 5.29, the cantilever tip reached and made contact with the cell surface at point B. When approaching the cell, the force value decreased until

it reached a maximal force value of at point C. The point at which the cantilever stabilized and finished the adhesion measurement was at point A. The displacement of the cantilever between the upper and lower boundary adhesion regions indicates the adhesion interval.

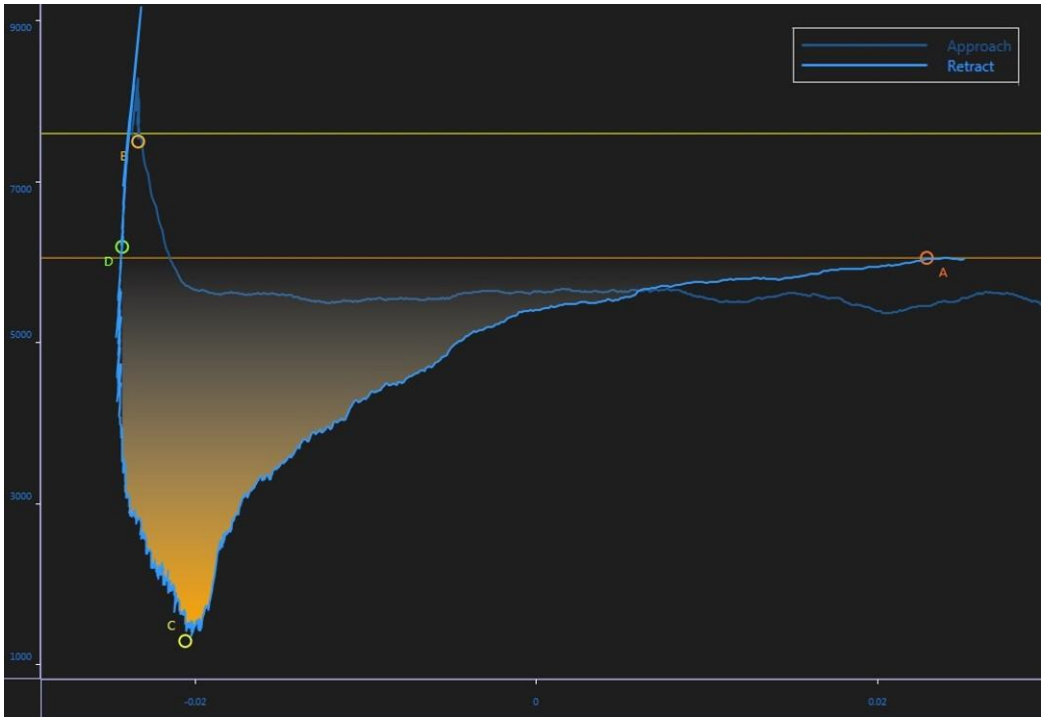

Figure 5.27: **Force-Distance Curve of a Completely Detached SH-SY5Y Cell.** Point A refers to the detachment or the upper boundary of the adhesion region. B indicates the point at which the tip makes contact with the surface. C is the point of maximal adhesion force. D is the lower boundary of the adhesion region. The highlighted yellow area represents the detachment work done during the retraction process.

Before detaching the cells and measuring their corresponding adhesion forces, sensitivity measurements were performed on empty areas of the substrate. The recorded sensitivity is dependent on the sample of interest and greatly changes between different samples. The recorded forces and measurements done are all dependent on the sensitivity measured for the corresponding substrate. The sensitivity of the control well tissue culture was recorded to be 1.21 x $10^{-}6$ m/V. That of the polyimide substrate with a 15 nm average surface roughness value was at 5.60 x $10^{-}5$ m/V.

The contact time of the cantilever to the cell surface while exerting an underpressure was set to be at 5 seconds. Figure 5.28 shows the same force-distance curve

as in Figure 5.29 with respect to time in seconds. At the point of contact, the force greatly increases and quickly decreases. It then increases with the increase in contact time until it reaches its highest value just before retraction.

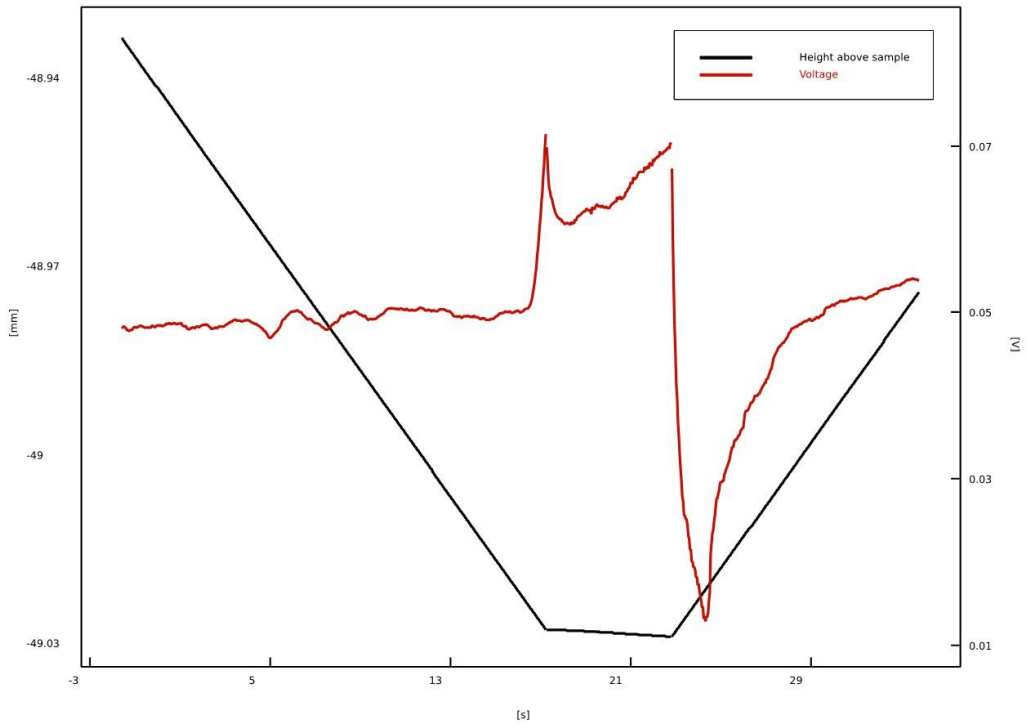

Figure 5.28: **Force-Time Curve of a Detached SH-SY5Y Cell.** The plot in black shows the height position variations (in mm) of the cantilever tip above the sample vs. time (in s). The curve in red shows the recorded voltage (in mV) of the cantilever tip during approach and retraction.

Several adhered SH-SY5Y cells were successfully detached from each of the control and polyimide samples. The adhesion forces and parameters were successfully measured for 13 cells on the control sample and 13 cells on the polyimide substrate, and their corresponding detachment videos were recorded. Each cell showed a distinct behavior response during detachment. Each of the figures 5.29 and 5.30 show 6 Force-Distance curves corresponding to 6 detached SH-SY5Y cells on control and polyimide, respectively, during retraction of the cantilever. From the graphs, the magnitude of the recorded adhesion force was higher in cells adhered to the polyimide substrates. The adhesion intervals were also higher in the polyimide samples. The curve shapes were different between the two samples

and between two cells on the same sample.

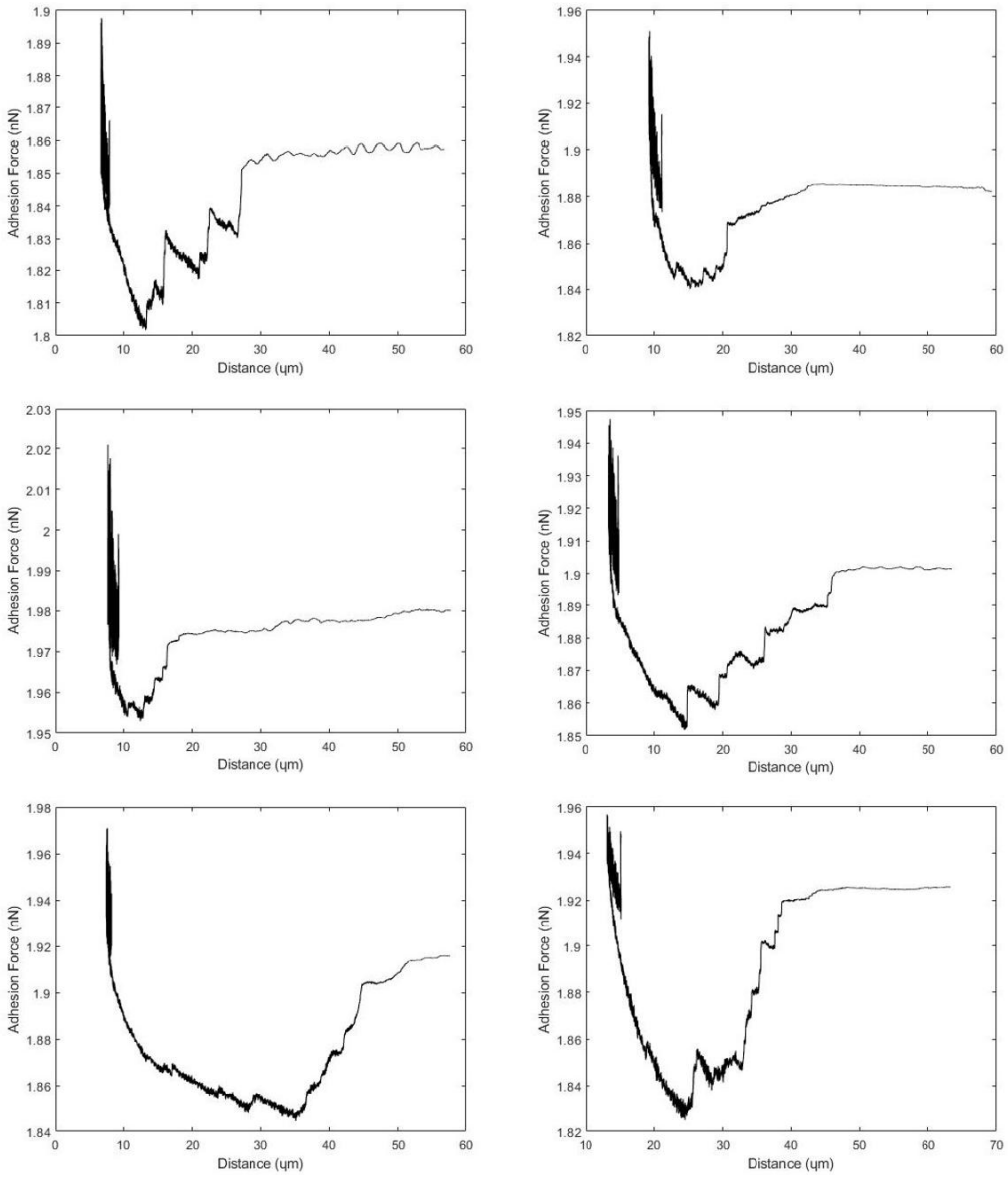

Figure 5.29: **Force-Distance Curves of Detached SH-SY5Y cells on Tissue Culture Plastic.** The plots represent the retraction phase of the cantilever.

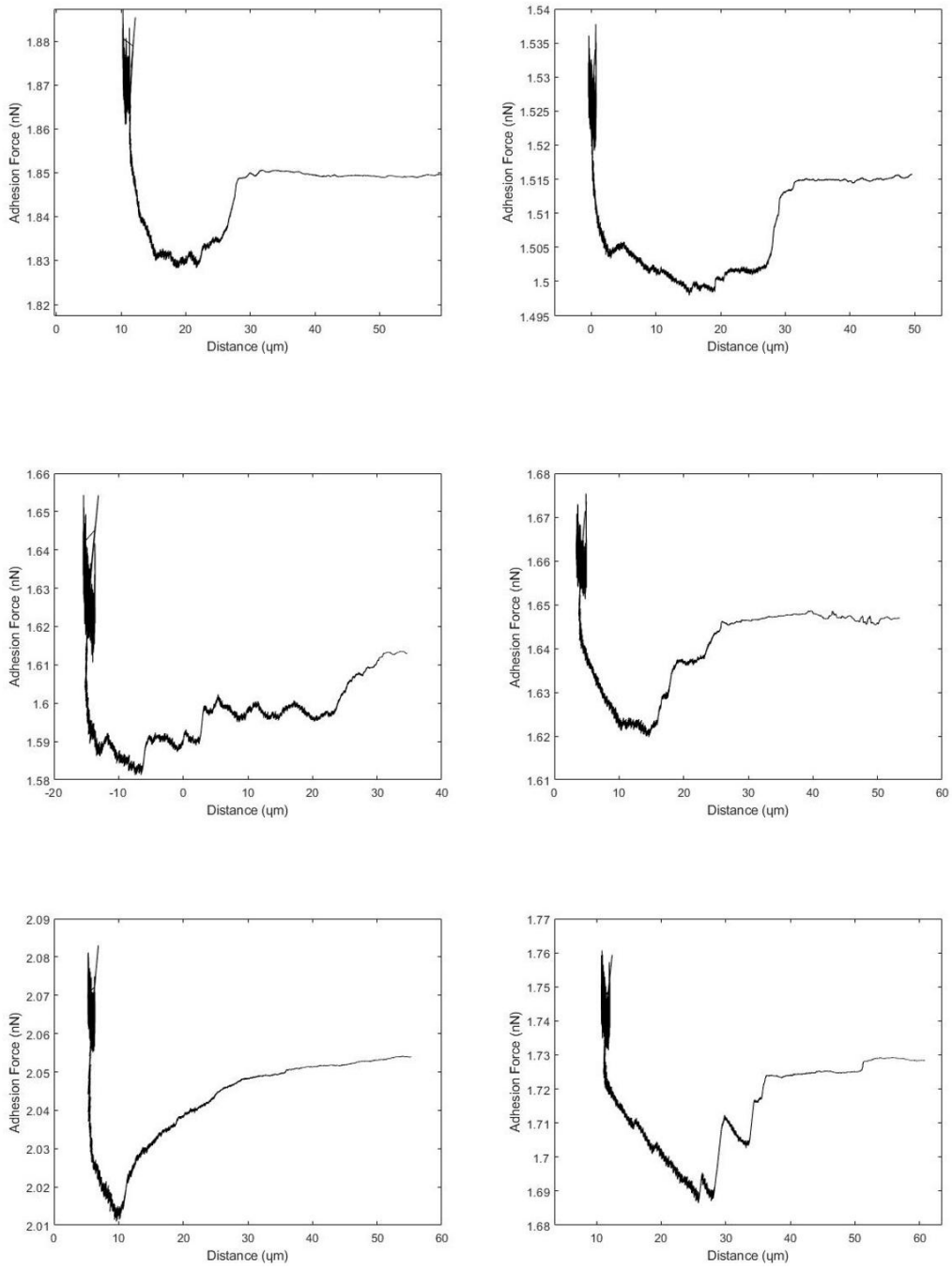

Figure 5.30: **Force-Distance Curves of Detached SH-SY5Y cells on Polyimide Substrate** with 15 nm average roughness. The plots represent the retraction phase of the cantilever.

From the exported data, several parameters were linearly correlated to demonstrate the relationship between the adhesion characteristic values and provide valuable information regarding the cell-to-substrate adhesion behaviors. Investigations were made to validate the correlation between adhesion force, maximal force, maximal distance, adhesion energy and cell area.

The maximal adhesion force was correlated with the maximal distance from the surface at which the maximal force is applied. As seen in Figure 5.31 (a), cells of higher maximal adhesion forces require greater maximal distance traveled. However, this relation is seen to be much stronger in the case of the SH-SY5Y cells adhered to the polyimide substrate, as in Figure 5.31 (b).

The recorded adhesion force values were correlated with their corresponding adhesion interval in Figure 5.32. In both samples, higher adhesion forces required higher adhesion intervals. As the adhesion interval increased, the adhesion force also increased. Since the specified retraction distance during measurement was chosen at 50 μ, the maximal interval distance recorded had a value of 50 50 μ.

Adhesion force and energy values were also investigated for correlation. Figure 5.33 shows that higher adhesion force values yielded higher adhesion energy values in both control and polyimide samples.

With image analysis, we were able to determine the cell area of the selected SH-SY5Y cells. Figures 5.34 (a) and (b) both show a good correlation relationship between cell area and maximal force. At greater maximal adhesion force values, the detached cells had a larger cell area. This relationship was found in the control and polyimide samples.

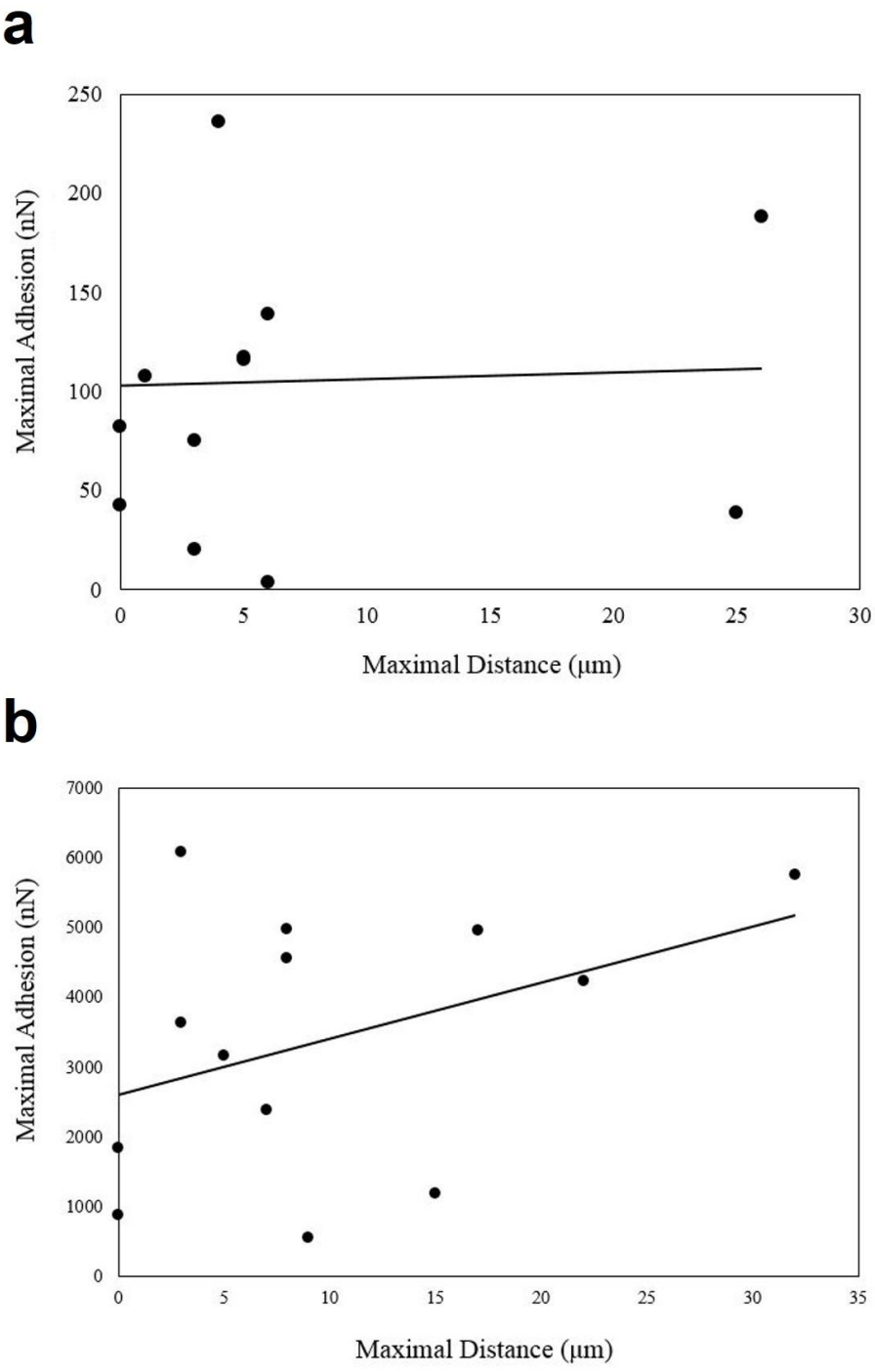

Figure 5.31: **Force-Distance correlation of single SH-SY5Y cells** on (a) tissue culture plastic and (b) polyimide substrate with 15 nm average roughness.

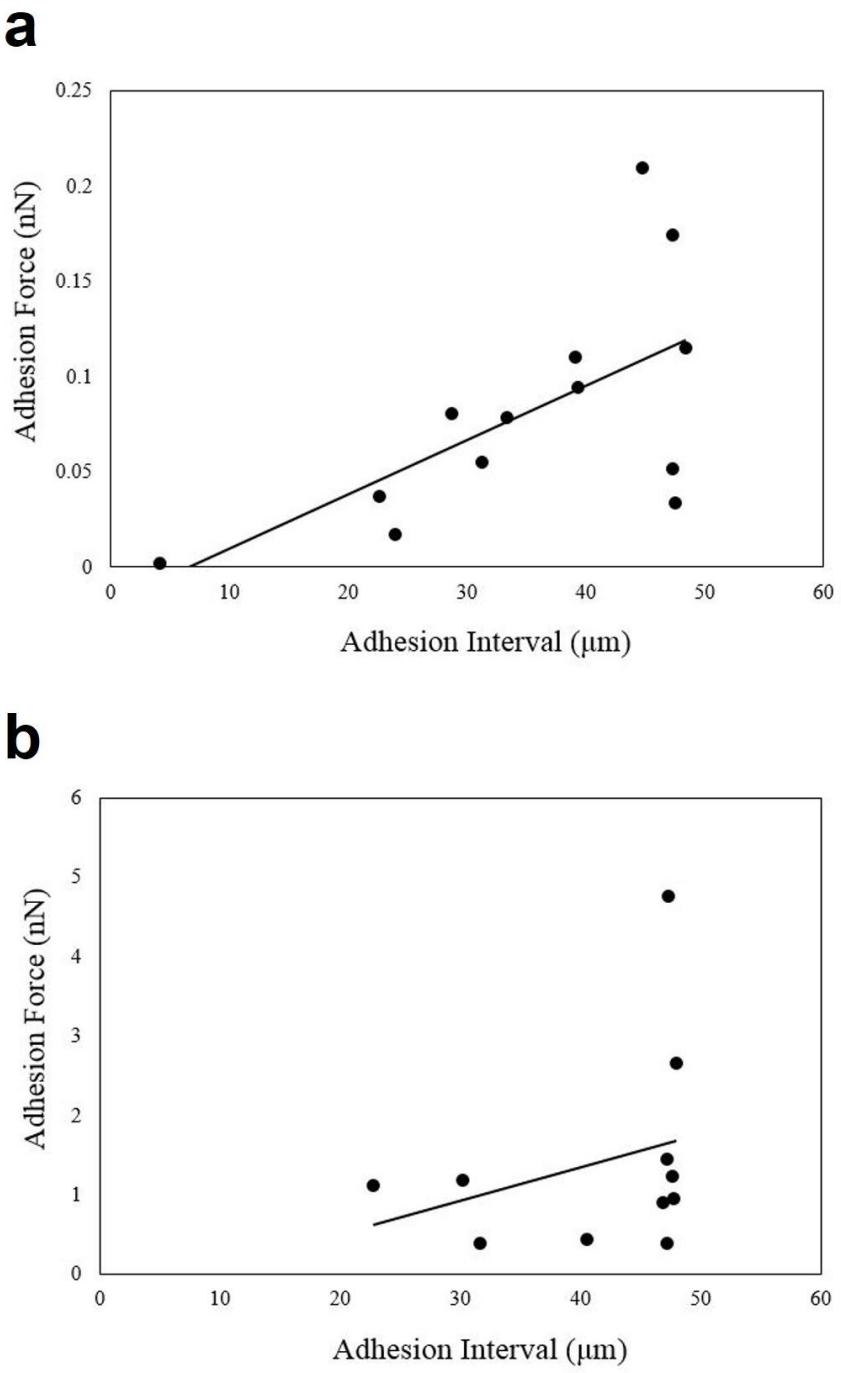

Figure 5.32: **Linear correlation of Force-Interval values of single SH-SY5Y cells** on (a) tissue culture plastic and (b) polyimide substrate with 15 nm average roughness.

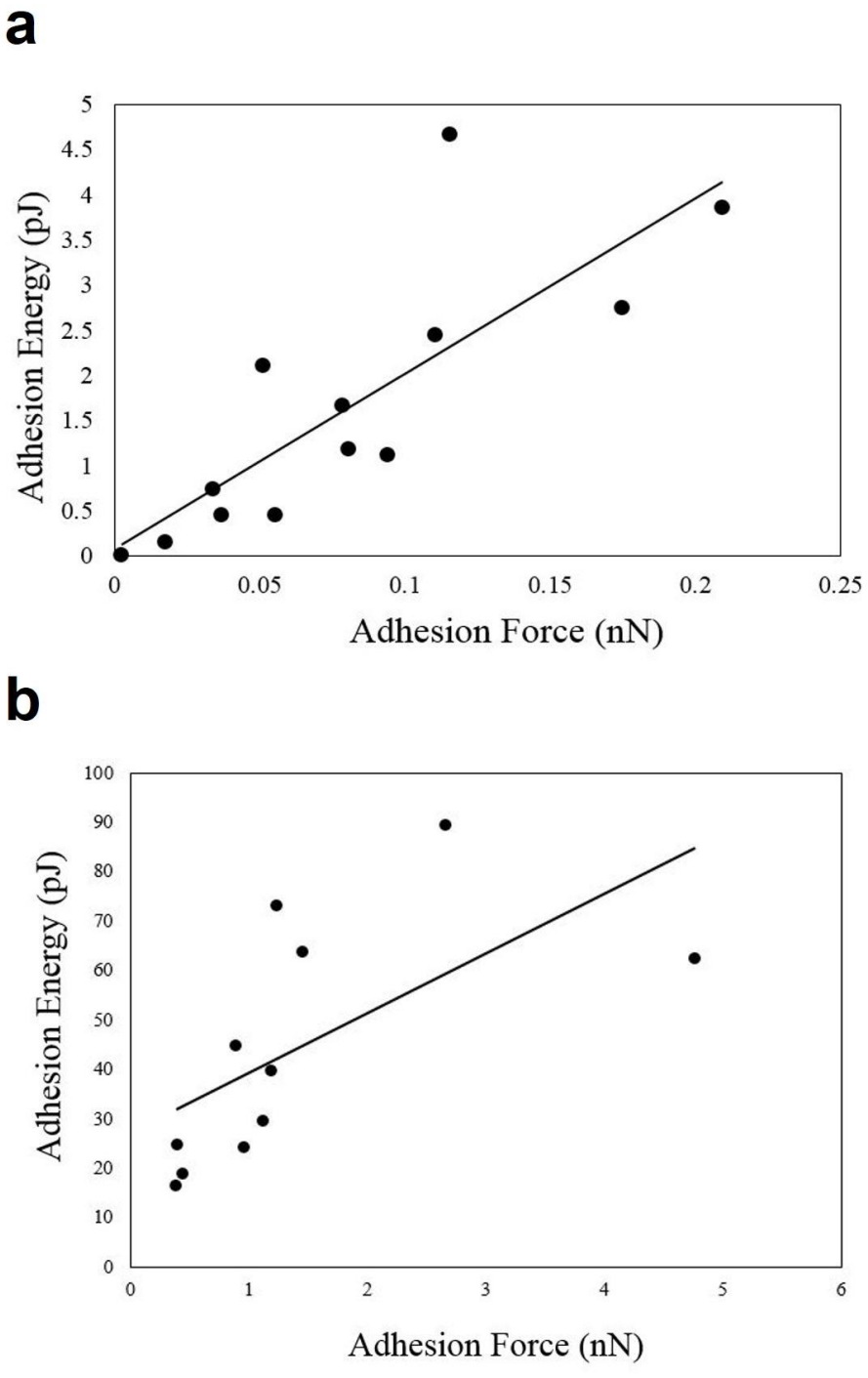

Figure 5.33: **Linear correlation of Force-Energy values of single SH-SY5Y cells** on (a) tissue culture plastic and (b) polyimide substrate with 15 nm average roughness.

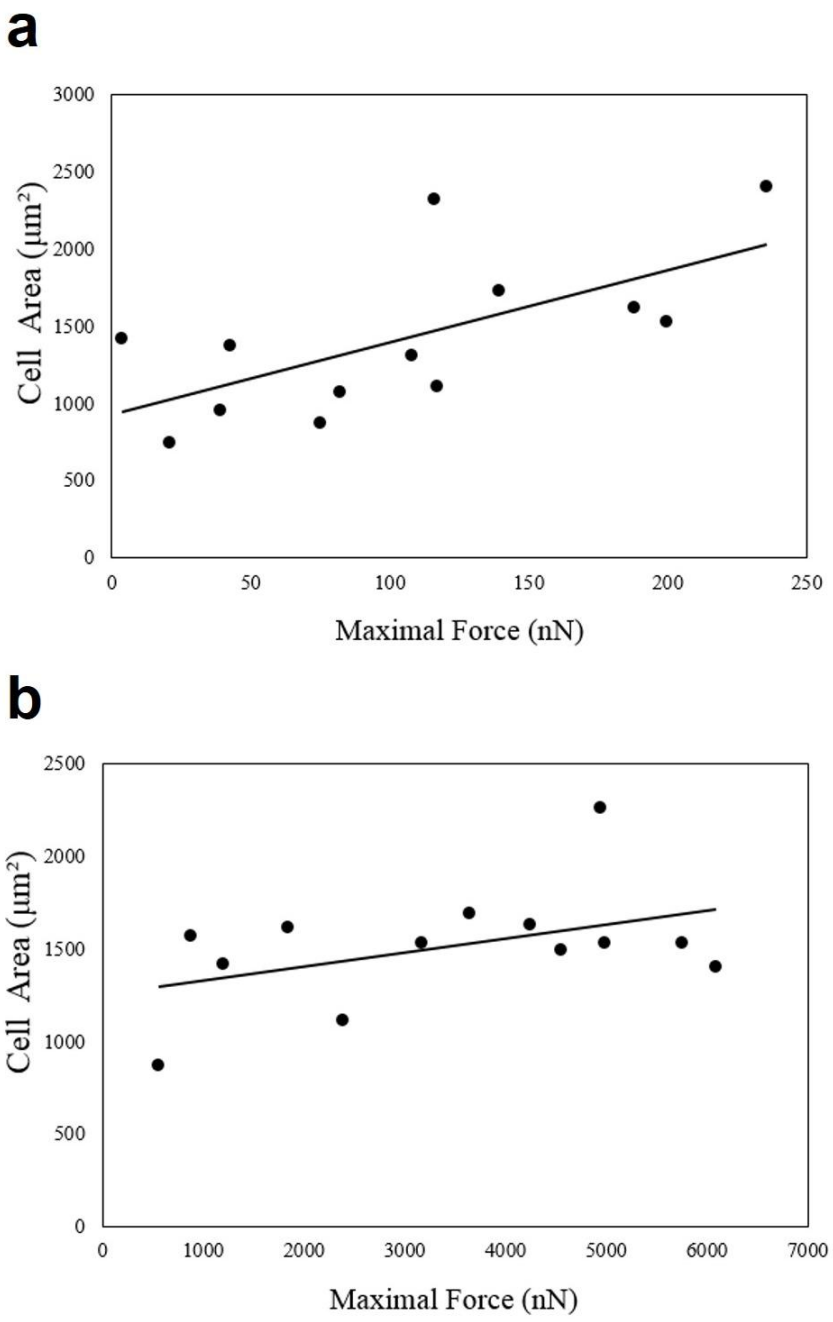

Figure 5.34: **Linear correlation of Force–Cell Area values of single SH-SY5Y cells** on (a) tissue culture plastic and (b) polyimide substrate with 15 nm average roughness.

Chapter 6

Discussion

6.1 Polyimide Surface Roughness and Wettability after Plasma

In this work, we were able to study the effect of plasma treating polyimide on the wettability and roughness of the surface. Only a few minutes of oxygen plasma were enough to lower the contact angle to negligible values. Low contact values correspond to a hydrophilic surface which can be correlated to a high surface energy. Since water has the highest surface tension, the contact angle measurements of water drops can be useful for the interpretation of the affinity interaction between the substrate and the cell in culture. However, we found that the contact angles change a few days after oxygen plasma treatment. The contact angle of the modified polyimide samples was no longer dependent on the treatment parameters and increased in all substrates. Excluding the surface energy variable from the study allowed us to evaluate cell behavior changes in response to surface roughness.

By manipulating the power, vacuum pressure and duration parameters of the plasma etcher, we were to study their influence on the surface roughness. We were able to develop several substrates with a range of roughness values at the nanometer level and without deterioration of the polyimide material. Etching at the lowest possible vacuum pressure values, which are controlled by the oxygen gas flow rates, produced polyimide substrates with the highest roughness values in the shortest amount of time. Since etching is a physical change to the sample surface, the surface roughness values averaged from several measurements were assumed to remain constant for the use in cell culture.

Etching polyimide for 30 minutes or more significantly changed its geometrical features, increased its surface roughness and, therefore, increased its surface area. This made it suitable for the study of cell adhesion to surface roughness

values at the low nanometer scale.

Roughening the polyimide surface through oxygen plasma provided a simple and convenient method for the development of nanorough polymer surfaces. The surface roughness of plasma-etched polyimide was more homogeneous than the calculated roughness values in graphene and PEDOT:PSS and were easier to manipulate and fine tune. In the case of polyimide, the samples that had highly variable roughness values were directly excluded from further experiments, and more homogeneously roughened surfaces were developed. Since the same polyimide surface can be re-treated to reach target roughness value, this approach is not material consuming.

6.2 Cell Viability

We were able to confirm the biocompatibility of the plasma-etched polyimide substrates and determine the SH-SY5Y cell preference with respect to the utilized nanorough substrates. The cells on all the substrates had relatively high viability percentages which made the substrates suitable for the use in cell culture. Substrates with average roughness values of around 8 nm encouraged the growth of SH-SY5Y cells, which can be confirmed by the calculated numbers in the supplementary tables. Both, the viability percentages and the count of viable cells, showed that the growth of SH-SY5Y cells was improved on those substrates. Moreover, the viability tests of the NHA on the polyimide substrates showed that they were able to grow and proliferate in a similar manner on the varied surface nano-roughness values.

From these experiments, we observed a distinct difference in the growth of SH-SY5Y cells and NHA on polyimide substrates with similar average roughness values. By finding a substrate with a surface roughness value that promotes the growth of one cell type and hinders the growth of another, we can better understand how a specific cell type interacts with the topography of its surrounding environment. When applied in neural interfaces, a device topography that improves the viability of neurons while discouraging that of glia shows better acceptance and allows neurons to survive over a longer period of time. It can be useful to perform these viability experiments on cultures that contain both cell types, neurons and glia, to demonstrate their interactions with each other and with the same underlying substrate to better represent their interactions inside the brain.

6.3 Cell-Substrate Adhesion

In our study, the assessment of the SH-SY5Y cell adhesion after 2 hours from seeding provided a good time point for the study of the effect of surface nanoroughness values on the cell behavior. After 2 hours from seeding, the majority of the SH-SY5Y cells would have attached to the substrates (that were not coated with adhesion proteins), but have not yet produced enough proteins and ECM components onto the substrate surface. Since the SH-SY5Y cells start changing phenotypic morphologies at passage numbers greater than 20, we were able to analyze two different behaviors to the nanorough substrates. SH-SY5Y cells at passages of 22-25 preferred adhering to substrates around 8 nm in average roughness values, which also agrees with the viability results. However, SH-SY5Y cells with late passage numbers preferred adhering to flat substrates. On the other hand, the adhesion experiments of NHA showed that they adhered more preferably to substrates with average roughness values of around 4 nm. NHA adhesion rapidly diminished on the selected substrates with higher surface roughness values.

We were able to find a surface roughness value that encourages neural adhesion and discourages glial adhesion at the same time. This selective adhesion principle can be useful in the application of neural interfaces, where neural adhesion is an important factor of device efficiency. We can conduct an experimental setup for studying the prolonged adhesion of primary neurons on a substrate and investigate changes in their adhesion versus changes in the adhesion of glia. Selective adhesion can also be helpful in cell sorting techniques. For that, we can study the initial adhesion of several cell types in one mix of cells to find an optimal surface roughness value for the initial adhesion of each desired cell type.

6.4 Single Cell-Substrate Adhesion Force Meaurement

We were able to successfully detach a cell from the surface and relate its detachment force to its strength of adhesion to the substrate without the need for trypsinization. We were able to consecutively detach several single cells and measure their corresponding cell-substrate adhesion forces in a fast and proper manner. The FluidFM was able to measure relatively high adhesion forces quicker than other common methods such as AFM. A negative applied pressure for a duration of only 5 seconds was enough for the cell detachment and its valid measurement. The selected pressure was a critical factor for the detaching of cells. The cells not completely detached were not measured again because they might have been deformed, and their adhesion response might have been altered.

In this study, we were able to quantify the adhesion behavior of SH-SY5Y cells on a substrate. Most importantly, we were able to demonstrate the difference in cellular adhesion responses in two different conditions. The magnitudes of the adhesion forces of SH-SY5Y cells on the polyimide substrate with an average of 15 nm were much higher than those on the regular tissue culture plastic. Their work needed for detachment increased with the increase of their detachment force, and the detachment force increased with the increase in adhesion interval, in both samples. Several force-distance curves described different detachment behaviors for the same cells in the same conditions. The measured adhesion force was observed to increase with the increase of cell area. This implies that when a cell spreads more, it adheres better to the underlying substrate, and more work is needed to detach it off the surface. Even though the measured cell area values of SH-SY5Y in both conditions were very similar, the maximal adhesion force of cells on the nano-rough polyimide substrate was much higher in magnitude. The nanoscale roughness of its surface provided more points of contact with the cell and encouraged cellular adhesion without disrupting the cell membrane.

6.5 Future Direction

Further experimental studies can be performed to evaluate the cellular adhesion responses of SH-SY5Y cells and NHA on surfaces with varying nano-roughness values. The adhesion experiments of SH-SY5Y cells need to also be evaluated at low passage numbers below 20 for cells that have not lost their neural-like morphology and phenotype. This helps better interpret the data in relation to neural cells. We can also conduct the same viability and adhesion experiments with the two cell types combined together on each substrate to mimic the conditions they intrinsically live in.

Moreover, the quantification of cell-substrate adhesion force on substrates with varying nano-roughness values would give a better understanding on how these cells interact with nanotopgraphy and provides relevant data for the advancement of adhesion-based cell separation techniques. This work can be extended to collect adhesion force measurements from different cell types and on different nano-roughened substrates to provide a clear reference for the biomechanical interactions between a cell and a substrate.

Chapter 7

Conclusion

Our study showed the impact of surface nanotopography on the viability and adhesion of neurons and glia. We found that glia and neurons exhibit a different adhesion response to surface roughness, which may allow for control over their selective adhesion. The choice of promoting the adhesion and subsequent growth of one cell type while hindering another would depend on the desired application. In neural interfaces, it is important to ensure proper neuronal adhesion while reducing glial adhesion for an efficient neuron/electrode junction.

Our results showed that surface roughness affected the contact area between the cell membrane and the substrate and yielded a change in cellular growth, proliferation, and adhesion. Neuroblastomas and glia showed a different response to surface roughness of the underlying substrate. Cells grown on 8nm nano-roughened substrates achieved maximum contact area (versus cells grown on 5nm rough substrates) with the surface and, therefore, had higher adhesion forces.

The property of nanotopography of a substrate was by itself sufficient in guiding biological responses. By simply varying the nanoscale features of a substrate, we were able to tune cell response to a substrate. The latter is useful in the development of biomaterials for brain implants. Also, the data collected in this study, along with future work, will broaden the understanding of mechanical cellular behavior and improve the design and development of electrodes.

Appendix A

Abbreviations

ABM	Astrocyte Basal Medium
AFM	Atomic Force Microscopy
CST	Critical Surface Tension
DAPI	4,6-Diamidino-2-Phenylindole
DHM	Digital Holographic Microscope
DMEM	Dulbecco's Modified Eagle Medium
FAK	Focal Adhesion Kinase
FBS	Fetal Bovine Serum
FluidFM	Fluid Force Microscopy
NHA	Normal Human Astrocytes
PBS	Phosphate Buffer Solution
PEDOT:PSS	Poly(3,4ethylenedioxythiophene):poly(styrenesulfonate)
PLL	Poly-L-Lysine
RF	Radio Frequency
SEM	Scanning Electron Microscope

Appendix B

Supplementary Material

B.1 Trypan Blue Exclusion Tests

B.1.1 48h Viability Test of SH-SY5Y Cells

control		coverglass		1.46 nm		4.03 nm		8.18 nm		12.09 nm	
Live	**Dead**	**Live**	**Dead**	**Live**	**Dead**	**Live**	**Dead**	**Live**	**Dead**	**Live**	**Dead**
11	2	10	1	10	1	10	1	17	1	7	1
8	0	9	1	11	1	5	0	6	1	15	1
10	0	6	0	17	3	8	1	10	0	3	0
6	0	10	1	10	1	7	0	4	1	6	1
5	0	7	2	9	0	15	1	12	0	5	1
6	1	8	1	12	2	9	0	9	0	12	2
11	1	7	1	11	1	10	2	11	1	10	0
9	1	12	3	10	0	8	1	6	0	9	1
12	2	11	1	8	0	3	1	10	1	8	0
9	1	9	2	5	0	9	1	14	1	14	1
7	2			2	0	18	0	7	1	9	0
9	2					12	3			17	1
19	1									11	1
122	**13**	**89**	**13**	**105**	**9**	**114**	**11**	**106**	**7**	**126**	**10**
%V	**90.3**	%V	**87.2**	%V	**92.1**	%V	**91.2**	%V	**93.8**	%V	**92.6**

Table B.1: **48h Viability Test of SH-SY5Y Cells Cultured on Polyimide Substrates with Varying Surface Nanoroughness Values.** The number of viable and non-viable cells were counted from several cytometer mounts. %V refers to the percentage of viable cells over the total number of cells. Passage number = 28.

control		coverglass		1.48 nm		4.14 nm		8.26 nm		12.18 nm		25.85 nm	
Live	**Dead**	**Live**	**Dead**	**Live**	**Dead**	**Live**	**Dead**	**Live**	**Dead**	**Live**	**Dead**	**Live**	**Dead**
17	4	10	3	25	1	14	2	9	0	14	2	24	4
23	3	8	2	6	2	9	1	8	0	20	1	10	0
13	2	7	2	14	1	13	4	22	1	8	1	10	1
9	3	8	2	10	1	8	2	10	0	11	0	14	2
19	1	17	6	17	1	11	3	16	1	13	1	14	1
21	1	11	2	8	2	10	4	11	1	67	4	41	1
14	1	17	5	7	2	9	3	38	1	8	1	12	0
10	2	22	3	10	1	11	3	26	3	11	1	13	2
18	6	26	3	7	2	16	4	7	1	12	1	9	1
16	5	19	2	13	2	8	3	8	0	9	1	13	5
20	4	10	0	27	3	11	3	6	1	9	1	9	1
7	0	10	1	13	1	9	2	7	0	12	0	8	0
5	1	5	3	17	4	12	4	31	2	11	1	12	2
41	4	19	1	13	3	41	5	13	4	8	0	22	1
		13	1	13	2	9	1	31	3	12	0	15	1
		15	2	36	2	16	3					15	3
						8	1						
233	**37**	**217**	**38**	**236**	**30**	**215**	**48**	**243**	**18**	**225**	**15**	**241**	**25**
%V	**86.3**	%V	**85.1**	%V	**88.7**	%V	**81.7**	%V	**93.1**	%V	**93.8**	%V	**90.6**

Table B.2: **48h Viability Test of SH-SY5Y Cells Cultured on Polyimide Substrates with Varying Surface Nanoroughness Values**The number of viable and non-viable cells were counted from several cytometer mounts. %V refers to the percentage of viable cells over the total number of cells. Passage number = 29.

Bibliography

[1] A. K. Howe, A. E. Aplin, and R. Juliano, "Anchorage-dependent erk signaling–mechanisms and consequences," *Current opinion in genetics & development*, vol. 12, no. 1, pp. 30–35, 2002.

[2] C. K. Miranti and J. S. Brugge, "Sensing the environment: a historical perspective on integrin signal transduction," *Nature cell biology*, vol. 4, no. 4, pp. E83–E90, 2002.

[3] P. J. Reddig and R. L. Juliano, "Clinging to life: cell to matrix adhesion and cell survival," *Cancer and Metastasis Reviews*, vol. 24, no. 3, pp. 425–439, 2005.

[4] T. F. Didar and M. Tabrizian, "Adhesion based detection, sorting and enrichment of cells in microfluidic lab-on-chip devices," *Lab on a Chip*, vol. 10, no. 22, pp. 3043–3053, 2010.

[5] K. W. Kwon, S. S. Choi, S. H. Lee, B. Kim, S. N. Lee, M. C. Park, P. Kim, S. Y. Hwang, and K. Y. Suh, "Label-free, microfluidic separation and enrichment of human breast cancer cells by adhesion difference," *Lab on a Chip*, vol. 7, no. 11, pp. 1461–1468, 2007.

[6] Y. Nam, "Material considerations for in vitro neural interface technology," *MRS bulletin*, vol. 37, no. 6, pp. 566–572, 2012.

[7] Y. Fan, F. Cui, L. Chen, Y. Zhai, Q. Xu, and I. Lee, "Adhesion of neural cells on silicon wafer with nano-topographic surface," *Applied surface science*, vol. 187, no. 3-4, pp. 313–318, 2002.

[8] Y. Fan, F. Cui, S. Hou, Q. Xu, L. Chen, and I.-S. Lee, "Culture of neural cells on silicon wafers with nano-scale surface topograph," *Journal of neuroscience methods*, vol. 120, no. 1, pp. 17–23, 2002.

[9] W. M. Grill and W. Reichert, "Signal considerations for chronically implanted electrodes for brain interfacing," *Indwelling neural implants: Strategies for contending with the in vivo environment*, pp. 42–58, 2008.

[10] J. W. Salatino, K. A. Ludwig, T. D. Kozai, and E. K. Purcell, "Glial responses to implanted electrodes in the brain," *Nature biomedical engineering*, vol. 1, no. 11, p. 862, 2017.

[11] J. P. Frampton, M. R. Hynd, M. L. Shuler, and W. Shain, "Effects of glial cells on electrode impedance recorded from neural prosthetic devices in vitro," *Annals of biomedical engineering*, vol. 38, no. 3, pp. 1031–1047, 2010.

[12] S. F. Cogan, K. A. Ludwig, C. G. Welle, and P. Takmakov, "Tissue damage thresholds during therapeutic electrical stimulation," *Journal of neural engineering*, vol. 13, no. 2, p. 021001, 2016.

[13] R. A. Green, N. H. Lovell, G. G. Wallace, and L. A. Poole-Warren, "Conducting polymers for neural interfaces: challenges in developing an effective long-term implant," *Biomaterials*, vol. 29, no. 24-25, pp. 3393–3399, 2008.

[14] A. Koklu, A. C. Sabuncu, and A. Beskok, "Rough gold electrodes for decreasing impedance at the electrolyte/electrode interface," *Electrochimica acta*, vol. 205, pp. 215–225, 2016.

[15] N. Joye, A. Schmid, and Y. Leblebici, "An electrical model of the cell-electrode interface for high-density microelectrode arrays," in *2008 30th Annual International Conference of the IEEE Engineering in Medicine and Biology Society*, pp. 559–562, IEEE, 2008.

[16] V. Pollak, "Impedance measurements on metal needle electrodes," *Medical and biological engineering*, vol. 12, no. 5, pp. 606–612, 1974.

[17] A. R. Harris, P. J. Molino, R. M. Kapsa, G. M. Clark, A. G. Paolini, and G. G. Wallace, "Correlation of the impedance and effective electrode area of doped pedot modified electrodes for brain–machine interfaces," *Analyst*, vol. 140, no. 9, pp. 3164–3174, 2015.

[18] J. Black, *Biological performance of materials: fundamentals of biocompatibility*. Crc Press, 2005.

[19] J. J. Green and J. H. Elisseeff, "Mimicking biological functionality with polymers for biomedical applications," *Nature*, vol. 540, no. 7633, pp. 386–394, 2016.

[20] W.-K. Oh, O. S. Kwon, and J. Jang, "Conducting polymer nanomaterials for biomedical applications: cellular interfacing and biosensing," *Polymer Reviews*, vol. 53, no. 3, pp. 407–442, 2013.

[21] U. A. Aregueta-Robles, A. J. Woolley, L. A. Poole-Warren, N. H. Lovell, and R. A. Green, "Organic electrode coatings for next-generation neural interfaces," *Frontiers in neuroengineering*, vol. 7, p. 15, 2014.

[22] L. W. McKeen, *Film properties of plastics and elastomers*. William Andrew, 2017.

[23] W. W. Wright and M. Hallden-Abberton, "Polyimides," *Ullmann's Encyclopedia of Industrial Chemistry*, 2000.

[24] B. Rubehn and T. Stieglitz, "In vitro evaluation of the long-term stability of polyimide as a material for neural implants," *Biomaterials*, vol. 31, no. 13, pp. 3449–3458, 2010.

[25] P. J. Rousche, D. S. Pellinen, D. P. Pivin, J. C. Williams, R. J. Vetter, and D. R. Kipke, "Flexible polyimide-based intracortical electrode arrays with bioactive capability," *IEEE Transactions on biomedical engineering*, vol. 48, no. 3, pp. 361–371, 2001.

[26] S. Wurth, M. Capogrosso, S. Raspopovic, J. Gandar, G. Federici, N. Kinany, A. Cutrone, A. Piersigilli, N. Pavlova, R. Guiet, *et al.*, "Long-term usability and bio-integration of polyimide-based intra-neural stimulating electrodes," *Biomaterials*, vol. 122, pp. 114–129, 2017.

[27] D. A. Brownson and C. E. Banks, "The handbook of graphene electrochemistry," 2014.

[28] S. W. Hong, J. H. Lee, S. H. Kang, E. Y. Hwang, Y.-S. Hwang, M. H. Lee, D.-W. Han, and J.-C. Park, "Enhanced neural cell adhesion and neurite outgrowth on graphene-based biomimetic substrates," *BioMed research international*, vol. 2014, 2014.

[29] A. Bendali, L. H. Hess, M. Seifert, V. Forster, A.-F. Stephan, J. A. Garrido, and S. Picaud, "Purified neurons can survive on peptide-free graphene layers," *Advanced healthcare materials*, vol. 2, no. 7, pp. 929–933, 2013.

[30] A. Fabbro, D. Scaini, V. Leo?n, E. Va?zquez, G. Cellot, G. Privitera, L. Lombardi, F. Torrisi, F. Tomarchio, F. Bonaccorso, *et al.*, "Graphene-based interfaces do not alter target nerve cells," *ACS nano*, vol. 10, no. 1, pp. 615–623, 2016.

[31] N. P. Pampaloni, M. Lottner, M. Giugliano, A. Matruglio, F. D'Amico, M. Prato, J. A. Garrido, L. Ballerini, and D. Scaini, "Single-layer graphene modulates neuronal communication and augments membrane ion currents," *Nature nanotechnology*, vol. 13, no. 8, p. 755, 2018.

[32] M. R. Abidian, K. A. Ludwig, T. C. Marzullo, D. C. Martin, and D. R. Kipke, "Interfacing conducting polymer nanotubes with the central nervous system: chronic neural recording using poly (3, 4-ethylenedioxythiophene) nanotubes," *Advanced Materials*, vol. 21, no. 37, pp. 3764–3770, 2009.

[33] R. M. Owens and G. G. Malliaras, "Organic electronics at the interface with biology," *MRS bulletin*, vol. 35, no. 6, pp. 449–456, 2010.

[34] D. Khodagholy, J. N. Gelinas, T. Thesen, W. Doyle, O. Devinsky, G. G. Malliaras, and G. Buzsáki, "Neurogrid: recording action potentials from the surface of the brain," *Nature neuroscience*, vol. 18, no. 2, p. 310, 2015.

[35] Y. Sun, S. Lacour, R. Brooks, N. Rushton, J. Fawcett, and R. Cameron, "Assessment of the biocompatibility of photosensitive polyimide for implantable medical device use," *Journal of Biomedical Materials Research Part A: An Official Journal of The Society for Biomaterials, The Japanese Society for Biomaterials, and The Australian Society for Biomaterials and the Korean Society for Biomaterials*, vol. 90, no. 3, pp. 648–655, 2009.

[36] H. Puliyalil and U. Cvelbar, "Selective plasma etching of polymeric substrates for advanced applications," *Nanomaterials*, vol. 6, no. 6, p. 108, 2016.

[37] D. P. Dowling, I. S. Miller, M. Ardhaoui, and W. M. Gallagher, "Effect of surface wettability and topography on the adhesion of osteosarcoma cells on plasma-modified polystyrene," *Journal of biomaterials applications*, vol. 26, no. 3, pp. 327–347, 2011.

[38] W. Zhou, X. Zhong, X. Wu, L. Yuan, Z. Zhao, H. Wang, Y. Xia, Y. Feng, J. He, and W. Chen, "The effect of surface roughness and wettability of nanostructured tio2 film on tca-8113 epithelial-like cells," *Surface and Coatings Technology*, vol. 200, no. 20-21, pp. 6155–6160, 2006.

[39] M.-E. Vlachopoulou, G. Kokkoris, C. Cardinaud, E. Gogolides, and A. Tserepi, "Plasma etching of poly (dimethylsiloxane): Roughness formation, mechanism, control, and application in the fabrication of microfluidic structures," *Plasma Processes and Polymers*, vol. 10, no. 1, pp. 29–40, 2013.

[40] P. Decuzzi and M. Ferrari, "Modulating cellular adhesion through nanotopography," *Biomaterials*, vol. 31, no. 1, pp. 173–179, 2010.

[41] E. Biazar, M. Heidari, A. Asefnezhad, and N. Montazeri, "The relationship between cellular adhesion and surface roughness in polystyrene modified by microwave plasma radiation," *International journal of nanomedicine*, vol. 6, p. 631, 2011.

[42] F. D. Egitto, "Plasma etching and modification of organic polymers," *Pure and applied Chemistry*, vol. 62, no. 9, pp. 1699–1708, 1990.

[43] N. Agarwal, S. Ponoth, J. Plawsky, and P. Persans, "Roughness evolution in polyimide films during plasma etching," *Applied Physics Letters*, vol. 78, no. 16, pp. 2294–2296, 2001.

[44] Y. Nakamura, Y. Suzuki, and Y. Watanabe, "Effect of oxygen plasma etching on adhesion between polyimide films and metal," *Thin Solid Films*, vol. 290, pp. 367–369, 1996.

[45] I. Song and A. Dityatev, "Crosstalk between glia, extracellular matrix and neurons," *Brain research bulletin*, vol. 136, pp. 101–108, 2018.

[46] D. Hoffman-Kim, J. A. Mitchel, and R. V. Bellamkonda, "Topography, cell response, and nerve regeneration," *Annual review of biomedical engineering*, vol. 12, pp. 203–231, 2010.

[47] P. A. Janmey and C. A. McCulloch, "Cell mechanics: integrating cell responses to mechanical stimuli," *Annu. Rev. Biomed. Eng.*, vol. 9, pp. 1–34, 2007.

[48] M.-H. Kim, M. Park, K. Kang, and I. S. Choi, "Neurons on nanometric topographies: insights into neuronal behaviors in vitro," *Biomaterials Science*, vol. 2, no. 2, pp. 148–155, 2014.

[49] M. O'Toole, P. Lamoureux, and K. E. Miller, "A physical model of axonal elongation: force, viscosity, and adhesions govern the mode of outgrowth," *Biophysical journal*, vol. 94, no. 7, pp. 2610–2620, 2008.

[50] B. Alberts, D. Bray, J. Lewis, M. Raff, K. Roberts, and J. D. Watson, "Molecular biology ofthe cell," *GarlandPublishing, New York*, 1994.

[51] B. D. Khalil, S. Hanna, B. A. Saykali, S. El-Sitt, A. Nasrallah, D. Marston, M. El-Sabban, K. M. Hahn, M. Symons, and M. El-Sibai, "The regulation of rhoa at focal adhesions by stard13 is important for astrocytoma cell motility," *Experimental cell research*, vol. 321, no. 2, pp. 109–122, 2014.

[52] H. K. Kim, E. Kim, H. Jang, Y.-K. Kim, and K. Kang, "Neuron–material nanointerfaces: surface nanotopography governs neuronal differentiation and development," *ChemNanoMat*, vol. 3, no. 5, pp. 278–287, 2017.

[53] C. D. Reyes and A. J. García, "A centrifugation cell adhesion assay for high-throughput screening of biomaterial surfaces," *Journal of Biomedical Materials Research Part A: An Official Journal of The Society for Biomaterials, The Japanese Society for Biomaterials, and The Australian Society*

for Biomaterials and the Korean Society for Biomaterials, vol. 67, no. 1, pp. 328–333, 2003.

[54] V. Yashunsky, V. Lirtsman, M. Golosovsky, D. Davidov, and B. Aroeti, "Real-time monitoring of epithelial cell-cell and cell-substrate interactions by infrared surface plasmon spectroscopy," *Biophysical journal*, vol. 99, no. 12, pp. 4028–4036, 2010.

[55] C. Christophis, M. Grunze, and A. Rosenhahn, "Quantification of the adhesion strength of fibroblast cells on ethylene glycol terminated self-assembled monolayers by a microfluidic shear force assay," *Physical Chemistry Chemical Physics*, vol. 12, no. 17, pp. 4498–4504, 2010.

[56] C. Zhu, "Kinetics and mechanics of cell adhesion," *Journal of biomechanics*, vol. 33, no. 1, pp. 23–33, 2000.

[57] C. Franz and P.-H. Puech, "Atomic force microscopy: a versatile tool for studying cell morphology, adhesion and mechanics," *Cellular and Molecular Bioengineering*, vol. 1, no. 4, pp. 289–300, 2008.

[58] M. Sztilkovics, T. Gerecsei, B. Peter, A. Saftics, S. Kurunczi, I. Szekacs, B. Szabo, and R. Horvath, "Single-cell adhesion force kinetics of cell populations from combined label-free optical biosensor and robotic fluidic force microscopy," *Scientific reports*, vol. 10, no. 1, pp. 1–13, 2020.

[59] J. E. Sader and L. White, "Theoretical analysis of the static deflection of plates for atomic force microscope applications," *Journal of Applied physics*, vol. 74, no. 1, pp. 1–9, 1993.

[60] V. J. Morris, A. R. Kirby, and P. A. Gunning, *Atomic force microscopy for biologists*. World Scientific, 2009.

[61] O. Guillaume-Gentil, E. Potthoff, D. Ossola, C. M. Franz, T. Zambelli, and J. A. Vorholt, "Force-controlled manipulation of single cells: from afm to fluidfm," *Trends in biotechnology*, vol. 32, no. 7, pp. 381–388, 2014.

[62] P. Honarmandi, H. Lee, M. J. Lang, and R. D. Kamm, "A microfluidic system with optical laser tweezers to study mechanotransduction and focal adhesion recruitment," *Lab on a chip*, vol. 11, no. 4, pp. 684–694, 2011.

[63] A. A. Khalili and M. R. Ahmad, "A review of cell adhesion studies for biomedical and biological applications," *International journal of molecular sciences*, vol. 16, no. 8, pp. 18149–18184, 2015.

[64] D. Y. Fozdar, J. Y. Lee, C. E. Schmidt, and S. Chen, "Hippocampal neurons respond uniquely to topographies of various sizes and shapes," *Biofabrication*, vol. 2, no. 3, p. 035005, 2010.

[65] J. M. Bruder, A. P. Lee, and D. Hoffman-Kim, "Biomimetic materials replicating schwann cell topography enhance neuronal adhesion and neurite alignment in vitro," *Journal of Biomaterials Science, Polymer Edition*, vol. 18, no. 8, pp. 967–982, 2007.

[66] M. Noble, J. Fok-Seang, and J. Cohen, "Glia are a unique substrate for the in vitro growth of central nervous system neurons," *Journal of Neuroscience*, vol. 4, no. 7, pp. 1892–1903, 1984.

[67] A. T. Nguyen, S. R. Sathe, and E. K. Yim, "From nano to micro: topographical scale and its impact on cell adhesion, morphology and contact guidance," *Journal of Physics: Condensed Matter*, vol. 28, no. 18, p. 183001, 2016.

[68] M. Arnold, E. A. Cavalcanti-Adam, R. Glass, J. Blümmel, W. Eck, M. Kantlehner, H. Kessler, and J. P. Spatz, "Activation of integrin function by nanopatterned adhesive interfaces," *ChemPhysChem*, vol. 5, no. 3, pp. 383–388, 2004.

[69] S. P. Massia and J. A. Hubbell, "An rgd spacing of 440 nm is sufficient for integrin alpha v beta 3-mediated fibroblast spreading and 140 nm for focal contact and stress fiber formation.," *The Journal of cell biology*, vol. 114, no. 5, pp. 1089–1100, 1991.

[70] V. Brunetti, G. Maiorano, L. Rizzello, B. Sorce, S. Sabella, R. Cingolani, and P. Pompa, "Neurons sense nanoscale roughness with nanometer sensitivity," *Proceedings of the National Academy of Sciences*, vol. 107, no. 14, pp. 6264–6269, 2010.

[71] K. Parikh, S. Rao, H. Ansari, L. Zimmerman, L. Lee, S. Akbar, and J. Winter, "Ceramic nanopatterned surfaces to explore the effects of nanotopography on cell attachment," *Materials Science and Engineering: C*, vol. 32, no. 8, pp. 2469–2475, 2012.

[72] G. Marinaro, R. La Rocca, A. Toma, M. Barberio, L. Cancedda, E. Di Fabrizio, P. Decuzzi, and F. Gentile, "Networks of neuroblastoma cells on porous silicon substrates reveal a small world topology," *Integrative Biology*, vol. 7, no. 2, pp. 184–197, 2015.

[73] Y. Khung, G. Barritt, and N. Voelcker, "Using continuous porous silicon gradients to study the influence of surface topography on the behaviour of neuroblastoma cells," *Experimental Cell Research*, vol. 314, no. 4, pp. 789–800, 2008.

[74] V. Onesto, A. Accardo, C. Vieu, and F. Gentile, "Small-world networks of neuroblastoma cells cultured in three-dimensional polymeric scaffolds featuring multi-scale roughness," *Neural regeneration research*, vol. 15, no. 4, p. 759, 2020.

[75] E. Maffioli, C. Schulte, S. Nonnis, F. Grassi Scalvini, C. Piazzoni, C. Lenardi, A. Negri, P. Milani, and G. Tedeschi, "Proteomic dissection of nanotopography-sensitive mechanotransductive signaling hubs that foster neuronal differentiation in pc12 cells," *Frontiers in cellular neuroscience*, vol. 11, p. 417, 2018.

[76] D. Schubert and C. Whitlock, "Alteration of cellular adhesion by nerve growth factor," *Proceedings of the National Academy of Sciences*, vol. 74, no. 9, pp. 4055–4058, 1977.

[77] J. D. Foley, E. W. Grunwald, P. F. Nealey, and C. J. Murphy, "Cooperative modulation of neuritogenesis by pc12 cells by topography and nerve growth factor," *Biomaterials*, vol. 26, no. 17, pp. 3639–3644, 2005.

[78] D. Convertino, S. Luin, L. Marchetti, and C. Coletti, "Peripheral neuron survival and outgrowth on graphene," *Frontiers in neuroscience*, vol. 12, p. 1, 2018.

[79] S. P. Khan, G. G. Auner, and G. M. Newaz, "Influence of nanoscale surface roughness on neural cell attachment on silicon," *Nanomedicine: Nanotechnology, Biology and Medicine*, vol. 1, no. 2, pp. 125–129, 2005.

[80] V. Onesto, L. Cancedda, M. Coluccio, M. Nanni, M. Pesce, N. Malara, M. Cesarelli, E. Di Fabrizio, F. Amato, and F. Gentile, "Nano-topography enhances communication in neural cells networks," *Scientific reports*, vol. 7, no. 1, p. 9841, 2017.

[81] T. D. Nguyen and Y. Gu, "Investigation of cell-substrate adhesion properties of living chondrocyte by measuring adhesive shear force and detachment using afm and inverse fea," *Scientific reports*, vol. 6, p. 38059, 2016.

[82] K.-L. P. Sung, M. K. Kwan, F. Maldonado, and W. H. Akeson, "Adhesion strength of human ligament fibroblasts," 1994.

[83] H. Xie, M. Yin, W. Rong, and L. Sun, "In situ quantification of living cell adhesion forces: single cell force spectroscopy with a nanotweezer," *Langmuir*, vol. 30, no. 10, pp. 2952–2959, 2014.

[84] H. Kizil, M. O. Pehlivaner, and L. Trabzon, "Surface plasma characterization of polyimide films for flexible electronics," in *Advanced Materials Research*, vol. 970, pp. 132–135, Trans Tech Publ, 2014.